



HAL
open science

Synthesis, crystal structure and Hirshfeld surface analysis of copper(II) complexes: DNA- and BSA-binding, molecular modeling, cell imaging and cytotoxicity

Marzieh Anjomshoa, Masoud Torkzadeh-Mahani, Jan Janczak, Corrado Rizzoli, Mehdi Sahihi, Farangis Ataei, Monireh Dehkhodaei

► To cite this version:

Marzieh Anjomshoa, Masoud Torkzadeh-Mahani, Jan Janczak, Corrado Rizzoli, Mehdi Sahihi, et al.. Synthesis, crystal structure and Hirshfeld surface analysis of copper(II) complexes: DNA- and BSA-binding, molecular modeling, cell imaging and cytotoxicity. *Polyhedron*, 2016, 119, pp.23-38. 10.1016/j.poly.2016.08.018 . hal-04087474

HAL Id: hal-04087474

<https://uca.hal.science/hal-04087474>

Submitted on 3 May 2023

HAL is a multi-disciplinary open access archive for the deposit and dissemination of scientific research documents, whether they are published or not. The documents may come from teaching and research institutions in France or abroad, or from public or private research centers.

L'archive ouverte pluridisciplinaire **HAL**, est destinée au dépôt et à la diffusion de documents scientifiques de niveau recherche, publiés ou non, émanant des établissements d'enseignement et de recherche français ou étrangers, des laboratoires publics ou privés.



Distributed under a Creative Commons Attribution - NonCommercial - NoDerivatives 4.0 International License

Synthesis, crystal structure and Hirshfeld surface analysis of copper(II) complexes: DNA- and BSA-binding, molecular modeling, cell imaging and cytotoxicity

Marzieh Anjomshoa ^a, Masoud Torkzadeh-

Mahani ^a, Jan Janczak ^b, Corrado Rizzoli ^c, Mehdi Sahihi ^d, Farangis Ataei ^e, Monireh Dehkhoda ^e

^a

Department of Biotechnology, Institute of Science and High Technology and Environmental Sciences, Graduate University of Advanced Technology, Kerman, Iran

^b

Institute of Low Temperature and Structure Research, Polish Academy of Sciences, P.O. Box 1410, Okólna 2 Str., 50-950 Wrocław, Poland

^c

Department of Chemistry, University of Parma, Parco Area delle Scienze 17/A, I-43124 Parma, Italy

^d

Department of Chemistry, University of Isfahan, Isfahan 81746-73441, Iran

^e

Department of Biochemistry, Faculty of Biological Sciences, Tarbiat Modares University, Tehran, Iran

Abstract

In order to explore the structure–activity relationship of complexes, two copper(II) complexes, [Cu(dimethoxybpy)₂](PF₆)₂ (**1**) and [Cu(dimethylbpy)₂Cl]PF₆ (**2**) (dimethoxybpy is 4,4'-dimethoxy-2,2'-bipyridine and dimethylbpy is 4,4'-dimethyl-2,2'-bipyridine), have been synthesized and characterized by several physicochemical techniques. The single-crystal X-ray structures of **1** and **2** exhibit distorted square-planar and distorted square-pyramidal structure, respectively. The Hirshfeld surface analysis and the associated 2D fingerprint plots of **1** and **2** have been also studied to evaluate intermolecular interactions. The DNA binding properties of **1** and **2** have been investigated by absorption and emission spectra, viscosity, cyclic voltammetry, circular dichroism and competitive DNA–binding studies, which indicate that the

complexes interact with DNA through partial intercalation. The results of absorption and emission spectra, synchronous fluorescence and circular dichroism show that the complexes bind with BSA. The results exhibit that the complex **1** has stronger binding ability to DNA and BSA than the complex **2**. Molecular docking technique has been used to evaluate and understand the interaction mode of **1** and **2** with DNA and BSA. The *in vitro* cytotoxicity of the complexes against MCF-7, A-549 and HT-29 cell lines has been assayed by MTT method. The complexes exhibit significant cytotoxicity in cell lines with IC₅₀ values ranging from 1.5 to 53 μM. Based on the results of cytotoxicity, it would appear that the complex **2** has better cytotoxicity than the complex **1** under the same experimental conditions, suggesting that the hydrophobicity of methyl groups on the complex enhances the anticancer activity. The results of the microscopic analyses of cancer cells confirm the results of cytotoxicity.

Keywords

4,4'-Dimethoxy-2,2'-bipyridine

4,4'-Dimethyl-2,2'-bipyridine

Hirshfeld surface analysis

GelRed

Cell imaging

1. Introduction

According to the recent reports, cisplatin is one of the most widely used and world's best-selling metal-based anticancer drugs which binds to DNA and inhibits the division of cancer cells [1], [2]. The widespread success of cisplatin in the clinical treatment has placed metal-based drugs in the frontline in the fight against cancer, numerous mononuclear platinum(II) complexes have been synthesized and their anticancer activities carefully evaluated on appropriate biological models [3]. Unfortunately, in contrast to general expectations, most of the platinum(II) complexes investigated so far exhibit biological activities very similar to those of cisplatin thus, with no significant therapeutic advantage. Also, the cancers that can be treated with platinum drugs are very few, and the drugs suffer from side effects and resistance phenomena [1], [4]. Therefore,

development of new alternative strategies for treatment of cancers is immediately required by finding out new transition metal complexes based on different metals and ligands with an aim of reducing toxicity, enhancing specificity, and thereby enhancing the therapeutic efficacy through noncovalent binding with DNA [2]. However, design concepts for such drugs are still in their primary steps; mainly because an understanding of structure–activity relationships has not yet reached a level that allows providing general rules.

Much attention has been paid to copper complexes, as the best promising alternatives to platinum drugs as anticancer drugs because of their rich synthetic chemistry, rich variety of coordination complexes from four to six with oxidation states Cu(II) and Cu(I), multiple mechanisms of action that are distinct from those of platinum-based drugs and low systemic toxicity [5]. In contrast to exogenous platinum, copper is found in all living organisms and is a crucial trace element in redox chemistry, growth, and development. However, copper can also be toxic to cells, due to its redox activity and its affinity for binding sites that should be occupied by other metals. Thus, several families of copper complexes have been studied as potential antitumor agents in recent years [5], [6], [7]. Copper(II) polypyridyl complexes are an important class of biologically active drugs and very interesting compounds with wide range of biological actions. In recent years many authors have published their findings about these complexes [8], [9]. The planner heterocyclic molecule of 2,2'-bipyridine and its derivatives are a kind of polypyridyl ligands, which plays an important role both chemists and biochemists. Ruiz-Azuara synthesized a class of mixed-chelate, cationic complexes named Casiopeinas having general formula $[\text{Cu}(4,4'\text{-dimethyl-2,2'\text{-bipyridine})(\text{acetylacetonate})]\text{NO}_3$ and $[\text{Cu}(4,4'\text{-dimethyl-2,2'\text{-bipyridine})(\text{glycinato})]\text{NO}_3$ [10], [11]. In other reports, wide range of biological actions of Casiopeinas complexes have been investigated [12], [13]. Fei et al. reported synthesis, DNA binding and cytotoxic activity of two novel copper-2,2'-bipyridine complexes [14]. 2,2'-Bipyridine and its derivatives complexes have shown mainly antibacterial activity, good affinity in DNA binding, and anticancer activity against human cancer cells [15], [16], [17], [18].

We present in this article the synthesis and characterization of two Cu(II) complexes, $[\text{Cu}(\text{dimethoxybpy})_2](\text{PF}_6)_2$ (**1**) and $[\text{Cu}(\text{dimethylbpy})_2\text{Cl}]\text{PF}_6$ (**2**). The crystal structures of the complexes have been determined by X-ray crystallography. The biological properties of **1** and **2** have been studied, including: (i) the binding properties of **1** and **2** with DNA by UV–Vis absorption, fluorescence titration, viscosity, cyclic voltammetry (CV) and circular dichroism

studies (CD) (ii) competitive binding studies with GelRed (GR) by fluorescence spectroscopy in order to investigate the existence of a potential intercalation of **1** and **2** to DNA, (iii) the binding properties of **1** and **2** with BSA by UV–Vis absorption, fluorescence, synchronous and circular dichroism, (iv) the interaction of **1** and **2** with DNA and BSA by molecular docking, (v) microscopic analyses of the cancer cells treated with **1** and **2** using an inverted microscope without any treatment or staining and (vi) the *in vitro* cytotoxicity activity of **1** and **2** on the human carcinoma cell lines (MCF-7, A-549 and HT-29) by the MTT assay.

2. Experimental

2.1. Materials

All reagents and solvents were purchased commercially and used without further purification unless otherwise noted. Tris(hydroxymethyl)-aminomethane (Tris) and BSA were purchased from Merck. Fish sperm DNA (FS-DNA) and 4,4'-dimethoxy-2,2'-bipyridine were purchased from Acros. Solution of DNA in Tris buffer (5 mM Tris/50 mM NaCl) gave a ratio of UV absorbance at 260 and 280 nm, A_{260}/A_{280} , of 1.9, indicating that the DNA was sufficiently free of protein [19]. 4,4'-Dimethyl-2,2'-bipyridine was purchased from Alfa Aesar. GelRed was purchased from Biotium.

2.2. Physical measurements

Elemental analyses were performed using a costech 4010 elemental analyzer. Fourier transform infrared spectra were recorded on a FT-IR Bruker-Tensor 27 spectrometer. Electronic absorption spectra were recorded on a Mecasys Optizen 3220 UV spectrophotometer using quartz cells with a path length of 1 cm. Fluorescence emission intensity measurements were carried out using a Varian Cary Eclipse spectrophotometer. The electrochemical measurements were performed with an Autolab potentiostat/galvanostat. CD spectra were recorded on an Aviv spectropolarimeter, model 215 using a cylindrical cuvette with 0.1 cm path length.

2.3. Syntheses

2.3.1. Synthesis of [Cu(dimethoxybpy)₂](PF₆)₂ complex (1)

0.17 g (1 mmol) of CuCl₂·H₂O and 0.43 g (2 mmol) of dimethoxybpy were dissolved in 15 mL of ethanol and stirred for 5 h at room temperature. The product was obtained by addition of a saturated aqueous NH₄PF₆ solution. The blue product, [Cu(dimethoxybpy)₂](PF₆)₂, was collected by suction filtration, washed with cold water and ether and then air-dried. For further purification, the blue precipitate was recrystallized by slow evaporation of an acetonitrile/dioxane solution of the complex gave shiny blue single crystals suitable for crystallography in a yield of 75%. *Anal. Calc.* for C₂₄H₂₄CuN₄O₄P₂F₁₂ (MW = 785.95): C, 36.6; H, 3.05; N, 7.12. Found: C, 36.49; H, 3.25; N, 6.97%. IR (KBr, cm⁻¹): 1615(s) ν(C–N) and 838(s) ν(P–F); UV–Vis λ_{max}/nm (ε_{max} × 10³/mol⁻¹ cm⁻¹): 231 (68), 276 (22), 285 (21) and 297 (17).

2.3.2. Synthesis of [Cu(dimethylbpy)₂Cl]PF₆ complex (2)

The complex was prepared using a procedure similar to that for **1** by using dimethylbpy (2 mmol, 0.37 g) instead of dimethoxybpy. The blue product, [Cu(dimethylbpy)₂Cl]PF₆, was collected by suction filtration, washed with cold water and ether and then air-dried. For further purification, the blue precipitate was recrystallized by slow diffusion of diethyl ether into an acetonitrile solution of the complex gave shiny blue single crystals suitable for crystallography in a yield of 83%. *Anal. Calc.* for C₂₄H₂₄ClCuF₆N₄P (MW = 612.43): C, 47.02; H, 3.92; N, 9.14. Found: C, 47.26; H, 3.96; N, 9.28%. IR (KBr, cm⁻¹): 3070 (w) ν(C–H_{cycle}), 2924 (w) ν(C–H_{Me}), 1615(s) ν(C–N) and 838(s) ν(P–F); UV–Vis λ_{max}/nm (ε_{max} × 10³/mol⁻¹ cm⁻¹): 235 (34), 295 (29) and 306 (26).

2.4. X-ray crystallographic procedure

Single crystal X-ray diffraction measurements of **1** were carried out at 295 (2) K on a four-circle KUMA KM4 diffractometer equipped with a two-dimensional CCD area detector. Graphite monochromatised Mo-Kα radiation (λ = 0.71073 Å) and ω-scan technique with step Δω = 1° were used for data collection and **2** carried out at 294 K on a Bruker APEX-II CCD diffractometer equipped with graphite monochromated Mo Kα radiation (λ = 0.71073 Å). Data collection and reduction of **1** were performed using the *CrysAlis* software package [20] and **2** were performed

using the SADABS software [21]. The structures were solved by direct methods using SHELXT program [22] which revealed the positions of almost all non-hydrogen atoms. The remaining atoms were located from subsequent difference Fourier synthesis. The structure was refined using SHELXL-2014/7 program [23] with anisotropic thermal displacement parameters. The hydrogen atoms were refined using the riding model with isotropic thermal displacement parameters 20% greater than aromatic carbon atoms linked directly the H atoms, and 50% greater than for carbon atom of CH₃. Visualization of the structure of **1** was made with Diamond 3.0 program [24]. Molecular plots of **2** were obtained using the ORTEP-3 [25] and SCHAKAL-99 [26] programs.

2.5. DNA binding experiments

Concentrated stock solution of DNA was prepared by dissolving appropriate amount of DNA in a Tris buffer (containing 5 mM Tris/50 mM NaCl at pH 7.30) and filtering through a Millipore filter. The DNA concentration per nucleotide was determined by absorption spectroscopy using the molar absorption coefficient ($6600 \text{ M}^{-1} \text{ cm}^{-1}$) at 260 nm.

Concentrated stock solutions of **1** and **2** were prepared by dissolving them in a solvent mixture of DMSO – Tris/NaCl buffer at pH 7.3 and diluting suitably with the corresponding buffer to the required concentrations for all of the experiments. Complexes **1** and **2** are soluble at $2 \times 10^{-5} \text{ M}$ in Tris/NaCl buffer (5 mM Tris/50 mM NaCl, pH 7.30) containing 0.2% DMSO. The stability of complexes is important for biological studies. To confirm the stability of **1** and **2** in the buffer solution at room temperature, a UV–Vis study was performed. The spectral features of **1** and **2** exhibited no change in the position of absorption bands over a period of 24 h and no precipitation or turbidity was observed even after long storage at room temperature (at least 1 month after preparation). This suggests that **1** and **2** are completely stable under the experimental conditions.

The absorption titrations were performed at room temperature using a constant concentration of **1** and **2**, with an increasing concentration of DNA. The concentrations of **1** and **2** were $2 \times 10^{-5} \text{ M}$, and DNA was added at ranging from $3.4 \times 10^{-5} \text{ M}$ to $60 \times 10^{-5} \text{ M}$. UV–Vis spectra were recorded in the range of 225–350 nm about 8 min after each addition of DNA solution. The intrinsic binding constants, K_b , of **1** and **2** with DNA have been determined using the UV spectra.

In the fluorescence quenching experiments with DNA, the concentration of **1** and **2** was constant (4×10^{-5} M), while gradually increasing the concentration of DNA at ranging from 3×10^{-5} M to 27×10^{-5} M. The fluorescence emission spectra were recorded at three different temperatures (290, 300 and 310 K) in the wavelength range of 280–450 nm by exciting the complexes at 270 nm.

The DNA binding was probed with the help of viscosity measurements using an Ostwald viscometer. The viscosity of a DNA solution has been measured in the absence and presence of increasing amounts of **1** and **2**. In DNA viscosity measurements, DNA is dissolved in Tris buffer to prepare 5×10^{-4} M working solution. The complexes were added with increasing concentrations from 2×10^{-5} M to 15×10^{-5} M to reach the [complex]/[DNA] ratios range from 0.04 to 0.30. The flow time was measured at least 3 times with a digital stopwatch and the mean value was calculated. In accordance with the theory of Cohen and Eisenberg [27], the data were plotted as intrinsic viscosity, $(\eta/\eta_0)^{1/3}$ versus the ratio of complex to DNA. The ratio $(\eta/\eta_0)^{1/3}$ was calculated based on $(\eta = t_f - t_0)$, where η is the viscosity of DNA in the presence of the complex, t_f is the flow time of the experimental trial, t_0 is the flow time of buffer, and η_0 is the viscosity of DNA solution in the absence of the complex.

Competitive studies of **1** and **2** with GelRed have been investigated with fluorescence spectroscopy in order to examine whether they can displace GR from its DNA-GR system. The emission spectra of GR bound to DNA in the absence and presence of the complexes have been recorded for [GR] = 1×10^{-5} M, [DNA] = 1×10^{-4} M, and increasing amounts of the complexes from 4×10^{-6} M to 36×10^{-6} M to reach the [complex]/[GR] ratios range from 0.4 to 3.6. DNA was pretreated with GR in the ratio [DNA]:[GR] = 10:1 for 1 h at 27 °C to ensure that the interaction between DNA and GR is complete. Fluorescence emission spectra were recorded in the wavelength range of 540–750 nm by exciting the GR-DNA system at 520 nm.

For the CD experiments, the concentrations of DNA and the Cu(II) complexes were 5×10^{-5} M and 1×10^{-6} M, respectively. The spectra of DNA in the absence and presence of the complexes were recorded in the range of 220–300 nm at 25 °C. The solutions were incubated for 10 min after each addition and then its CD spectrum was recorded at 100 nm/min scan rate. The spectrum of Tris buffer was subtracted from sample spectra for data analysis.

CV measurements were recorded by keeping the concentration of **1** and **2** constant and addition of a solution of DNA. The supporting electrolyte was a buffer solution containing 5 mM Tris/10 mM

NaCl buffer (pH 7.2). All measurements were carried out in a single compartmental 15 mL electrolytic cell with three-electrode system comprising of a glassy carbon electrode (GCE) ($\Phi = 2$ mm) as the working electrode, a platinum wire as the auxiliary electrode and a Ag/AgCl as a pseudo reference electrode.

2.6. BSA binding experiments

Concentrated stock solution of BSA was prepared by dissolving the appropriate amount of BSA in a Tris buffer (containing 5 mM Tris/50 mM NaCl at pH 7.30). BSA concentration was determined spectrophotometrically by using $\lambda_{280} = 44300 \text{ M}^{-1}\text{cm}^{-1}$.

Absorption titration experiments were performed by keeping the BSA concentration constant ($15 \times 10^{-6} \text{ M}$), while gradually increasing the concentration of the complexes at ranging from $2 \times 10^{-6} \text{ M}$ to $14 \times 10^{-6} \text{ M}$. UV-Vis spectra were recorded in the range of 200–320 nm. The change in absorbance of the characteristic bands of the BSA at $\lambda_{\text{max}} = 230$ and 280 nm was recorded each time after titrant addition.

In the fluorescence titration experiments, a fixed concentration of BSA ($4 \times 10^{-6} \text{ M}$) was titrated by successive additions of the stock solution of **1** and **2** at ranging from $4 \times 10^{-6} \text{ M}$ to $32 \times 10^{-6} \text{ M}$. The fluorescence emission spectra were recorded at three different temperatures (290, 300 and 310 K). The fluorescence emission spectra were measured in the wavelength range of 290–420 nm with an excitation and emission wavelength at 280 and 344 nm, respectively.

For synchronous fluorescence spectra also, the same concentration of BSA and **1** and **2** were used and the spectra were measured at two different $\Delta\lambda$ (difference between the excitation and emission wavelengths of BSA) values such as 15 and 60 nm.

The effect of the complexes on the BSA secondary structure was recorded by measuring the CD spectra. For the CD experiments, the concentrations of BSA and the Cu(II) complexes were $2 \times 10^{-6} \text{ M}$ and $2 \times 10^{-6} \text{ M}$, respectively. The spectra of BSA in the absence and presence of **1** and **2** were recorded in the range of 200–260 nm at 25 °C using a bandwidth of 1 nm, a step interval of 1 nm, an average time of 0.5 s, and a slit width of 0.02 mm. The spectrum of Tris buffer was subtracted from sample spectra for data analysis.

2.7. Molecular dynamics simulation

The structure of DNA (PDB ID: 423D) with sequence d(ACCGACGTCGGT)₂ and BSA (PDB ID: 4F5S) were taken from the Protein Data Bank (<http://www.rcsb.org/pdb>) with the resolution of 1.60 and 2.47 Å, and the *r*-value of 0.206 and 0.259 for DNA and BSA, respectively. A 20 ns MD studies were carried out using the GROMACS 4.5.6 (University of Groningen, Netherlands) package [28], [29] and the GROMOS96 43a1 force field [30], [31]. The macromolecules were located in the cubic box with the periodic boundary conditions and the minimum distance between the macromolecules surface and the box was 1.0 nm. The box, filled with extended simple point charges (SPC), water molecules [32]. Energy minimization was done through using the steepest descent method. Then, the system was equilibrated for 100 ps at the temperature of 300 K. Finally, a 20 ns MD simulation was carried out at 1 bar and 300 K. A Berendsen thermostat [33] at 300 K, the particle mesh Ewald (PME) method [34], [35] for long range electrostatics, and a 9 Å cut off for van der Waals interactions and Coulomb interactions were used. The equation of motions was integrated by the leap-frog algorithm with the 2 fs time steps. The atomic coordinates were recorded to the trajectory file every 0.5 ps for later analysis. The stability of simulated systems was scanned using the root-mean-square deviations (RMSDs) of BSA and DNA with respect to their initial structures. The equilibrated conformation of the BSA and DNA were used for docking.

2.8. Molecular docking

Docking study was carried out to indicate the active binding site for **1** and **2**. The 3D structure of **1** and **2** were generated using the CIF file of their X-ray crystal structure. The CIF file was converted to the PDB format by using the Mercury software (<http://www.ccdc.cam.ac.uk/>) and missing hydrogen atoms and Gasteiger charges were added. Flexible-ligand docking was performed by Auto Dock 4.2 molecular-docking program using the implemented empirical free energy function and the Lamarckian Genetic Algorithm [36]. The Auto Grid was used to calculate Grids and a blind docking with 126 lattice points along X, Y, and Z axes was performed to find the active site of ligands to the biomacromolecules. After determination of the active site, the dimensions of the grid map were selected 60 points with a grid point spacing of 0.375 Å, to allow the ligand to rotate freely. 200 docking runs with 25 000 000 energy evaluations for each run were performed.

2.9. Cytotoxic activity assays

2.9.1. Cell culture

MCF-7 (human breast carcinoma), A-549 (human lung carcinoma) and HT-29 (human colon carcinoma) cells were obtained from the cell bank of the Pasteur Institute of Iran. These cells were maintained in an RPMI 1640 medium supplemented with 10% (v/v) heat-inactivated fetal bovine serum (FBS, Gibco), 2 mM of glutamine, and 1% penicillin streptomycin (Invitrogen) in 96 well culture plates, at 37 °C in a humidified atmosphere in the presence of 5% CO₂.

2.9.2. Assessment of cytotoxicity activity using MTT assay

The cancer cells were seeded at a density of 5×10^3 cells/well into sterile 96 well plates and incubated at 37 °C in a humidified 5% CO₂ incubator for 24 h. A stock solution of **1** and **2** was prepared in DMSO solvent and diluted with the cell culture medium. After 24 h, the cells were treated in triplicate with increasing concentrations of **1** and **2** (1, 10, 20, 30, 40 and 60 μM) and incubated for 24 h. A miniaturized viability assay using 3-(4,5-dimethylthiazol-2-yl)-2,5-diphenyl-2H-tetrazolium-bromide (MTT) was carried out according to the method described by Mosmann [37]. This method is commonly used to illustrate inhibition of cellular proliferation. Drug-treated cells were assayed by addition of 20 μL of 5 mg/ml MTT. Following incubation for 4 h at 37 °C, the overlying medium was aspirated with a syringe and 200 μL of DMSO was added to dissolve the formazan crystals. The cells were incubated and protected from light for 20 min at room temperature. Then, the cells were shaken for 2 min before reading by ELISA reader (Bio-Tek, Elx 808, Germany) at $\lambda = 545$ nm. The absorbance of each well converted to percentage of cell growth inhibition [38].

3. Results and discussion

3.1. Syntheses and characterization of the Cu(II) complexes

In order to explore the structure–activity relationship of complexes, two Cu(II) complexes, [Cu(dimethoxybpy)₂](PF₆)₂ (**1**) and [Cu(dimethylbpy)₂Cl]PF₆ (**2**), were synthesized by the reaction of CuCl₂·H₂O and two different 2,2'-bipyridine based ligands (4,4'-dimethoxy-2,2'-bipyridine and 4,4'-dimethyl-2,2'-bipyridine) in ethanol solution. Then, the complexes were

isolated as the hexafluorophosphate salt in aqueous solution. The complexes have been obtained in good yields and characterized by elemental analysis and FT-IR.

3.1.1. Crystal structure of $[\text{Cu}(\text{dimethoxybpy})_2](\text{PF}_6)_2$ (**1**)

The complex **1** crystallizes in centrosymmetric space group $Fddd$ of the orthorhombic system with 8 molecules per unit cell. X-ray single crystal analysis established that the asymmetric unit consist of one fourth of $[\text{Cu}(\text{dimethoxybpy})_2](\text{PF}_6)_2$ complex. The molecular structure of the complex **1** with the anisotropic displacement parameters is illustrated in Fig. 1. The crystallographic data of the complex are summarized in Table 1. The complex **1** consists of mononuclear $[\text{Cu}(\text{dimethoxybpy})_2]^{2+}$ cations and PF_6^- anions in the molar ratio 1:2, cations and anions having crystallographically imposed 222 and twofold symmetry, respectively. The copper atom of the $[\text{Cu}(\text{dimethoxybpy})_2]^{2+}$ cation is coordinated by four N atoms from two dimethoxybpy ligands forming a CuN_4 chromophore in a remarkably distorted square-planar geometry. The magnitude of this distortion can be expressed through the τ_4 index ($\tau_4 = (360 - (\beta + \alpha))/141$), (β and α are the two largest L–M–L angles [39], which for the complex results to be 0.41. The 4,4'-dimethoxy-2,2'-bipyridine ligands are almost planar, the dihedral angle between the pyridine rings being $7.7(2)^\circ$. The dihedral angle between the least-square mean planes through the ligands is $50.1(3)^\circ$. The Cu–N bond lengths are identical for symmetry reasons (Table 2).

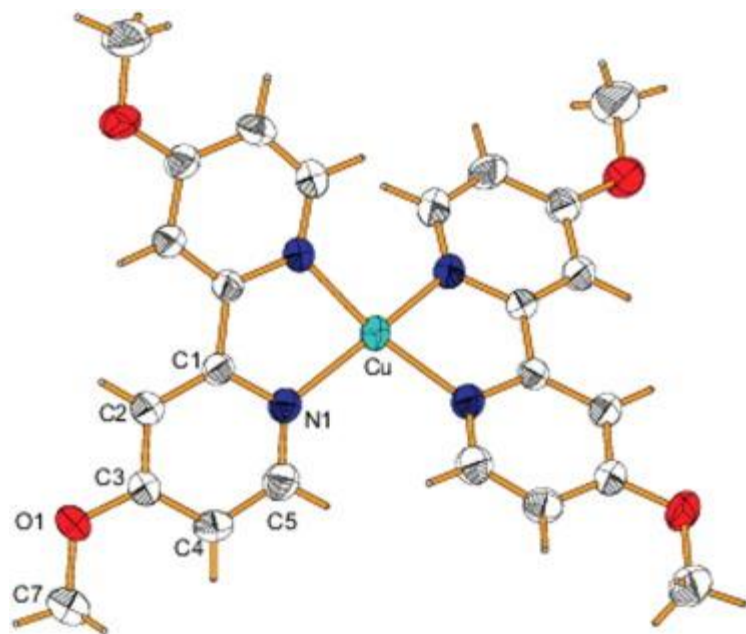


Fig. 1. The molecular structure of the complex **1** with labeling scheme of the asymmetric unit showing anisotropic displacement parameters at the 50% probability level. Counter anions (PF_6^-) have been emitted for more clarity. H atoms represent the circle with arbitrary radii.

Table 1. Crystal data and structure refinement for complexes **1** and **2**.

Complex	1	2
Chemical formula	$\text{C}_{24}\text{H}_{24}\text{CuN}_4\text{O}_4\text{P}_2\text{F}_{12}$	$\text{C}_{24}\text{H}_{24}\text{ClCuN}_4\text{P F}_6$
Formula weight	785.95	612.43
Radiation	Mo K_α ($\lambda = 0.71073 \text{ \AA}$)	Mo K_α ($\lambda = 0.71073 \text{ \AA}$)
Temperature (K)	295(2)	294(2)
Crystal size (mm^3)	$0.28 \times 0.23 \times 0.19$	$0.31 \times 0.15 \times 0.12$
Crystal system	Orthorhombic	Triclinic
Space group	<i>Fddd</i>	$\text{P}\bar{1}$
<i>Z</i>	8	2
<i>a</i> (\AA)	9.8268(4)	8.9077(7)
<i>b</i> (\AA)	13.1942(6)	10.9691(8)
<i>c</i> (\AA)	46.2535(16)	14.0476(11)
α ($^\circ$)	90	80.7843(11)
β ($^\circ$)	90	74.7995(11)
γ ($^\circ$)	90	82.0749(11)
<i>V</i> (\AA^3)	5997.1(4)	1300.82(17)
D_{calc} (g cm^{-3})	1.741	1.564
Absorption coefficient (μ) (mm^{-1})	0.949	1.068

Complex	1	2
Absorption correction	Multi-scan	Multi-scan
Collection ranges	$-12 \leq h \leq 10$; $-16 \leq k \leq 16$; $-58 \leq l \leq 59$	$-10 \leq h \leq 10$; $-13 \leq k \leq 13$; $-17 \leq l \leq 17$
Completeness	99.9% ($\theta = 27.60$)	99.9% ($\theta = 25.50$)
Reflections collected/unique	20279/1772	14761/4841
R_{int}	0.0250	0.0195
Data/restraints/parameters	1772/0/109	4841/0/338
$F(0\ 0\ 0)$	3160	622
θ (°)	2.65–28.25	1.51–25.50
Final R indices [$I > 2\sigma(I)$]	$R1^a = 0.0382$, $wR2^b = 0.0873$	$R1^a = 0.0403$, $wR2^b = 0.1148$
R indices (all data)	$R1^a = 0.0608$, $wR2^b = 0.0947$	$R1^a = 0.0420$, $wR2^b = 0.1162$
Largest difference peak and hole ($e\ \text{\AA}^{-3}$)	0.545 and -0.275	0.874 and -0.468

a

$$R1 = \frac{\sum ||F_o| - |F_c||}{\sum F_o}$$

b

$$wR2 = \left\{ \frac{\sum [w(F_o^2 - F_c^2)^2]}{\sum wF_o^4} \right\}^{1/2} w = 1/[\sigma^2(F_o^2) + (aP)^2 + bP] \quad \text{where } a = 0.0549$$

and $b = 3.4507$ for **1** and $a = 0.0653$ and $b = 0.9349$ for **2**, and $P = (F_o^2 + 2F_c^2)/3$.

Table 2. Selected bond lengths (Å) and bond angles (°) for complexes **1** and **2**.

1	2		
<i>Bond lengths</i> (Å)			
Cu–N1 (x4) ^a	1.9699(16)	Cu1—Cl1	2.2576(8)
P—F1 (x2) ^a	1.5854(15)	Cu1—N4	1.994(2)

1		2	
P—F2 (x2) ^a	1.513(2)	Cu1—N3	2.073(2)
P—F3 (x2) ^a	1.482(2)	Cu1—N2	1.988(2)
		Cu1—N1	2.149(2)
<i>Bond angles (°)</i>			
N1—Cu—N1 ⁱ	83.21(9)	N2—Cu—Cl1	91.83(6)
N1—Cu—N1 ⁱⁱ	103.98(9)	N4—Cu—Cl1	95.05(7)
N1—Cu—N1 ⁱⁱⁱ	151.24(10)	N4—Cu—N2	173.02(9)
F1—P—F2	88.14(11)	N1—Cu—Cl1	116.23(6)
F1—P—F3	90.27(13)	N3—Cu—Cl1	142.56(6)
F1—P—F3 ^{iv}	90.73(12)	N2—Cu—N1	78.91(8)
F1—P—F2 ^{iv}	90.79(12)	N4—Cu—N3	79.51(9)
F1—P—F1 ^{iv}	178.48(15)	N3—Cu—N1	101.19(8)
		N3—Cu—N2	94.30(8)
		N4—Cu—N1	99.02(8)

a

symmetry operators generate the equivalent bonds; symmetry code: (i) $-x + 1/4$, $-y + 5/4$, z ; (ii) x , $-y + 5/4$, $-z + 5/4$; (iii) $-x + 1/4$, y , $-z + 5/4$; (iv) $-x + 3/4$, $-y + 3/4$, z .

The crystal packing is mainly determined by the ionic interactions between the $[\text{Cu}(\text{dimethoxybpy})_2]^{2+}$ cations and PF_6^- anions and by van der Waals forces. In addition, weak interactions between oppositely polarized H atoms of the cations and F atoms of the PF_6^- anions (C—H \cdots F contacts with H \cdots F distances between 2.38 and 2.66 Å) forming pseudo-two-dimensional layers parallel to (1 1 0) plane are observed (Fig. 2A). Neighboring layers related by the d plane perpendicular to the c -axis weakly interact only by the van der Waals forces (Fig. 2B) and therefore the (1 0 0) plane is a cleavage plane of the $[\text{Cu}(\text{dimethoxybpy})_2](\text{PF}_6)_2$ crystals.

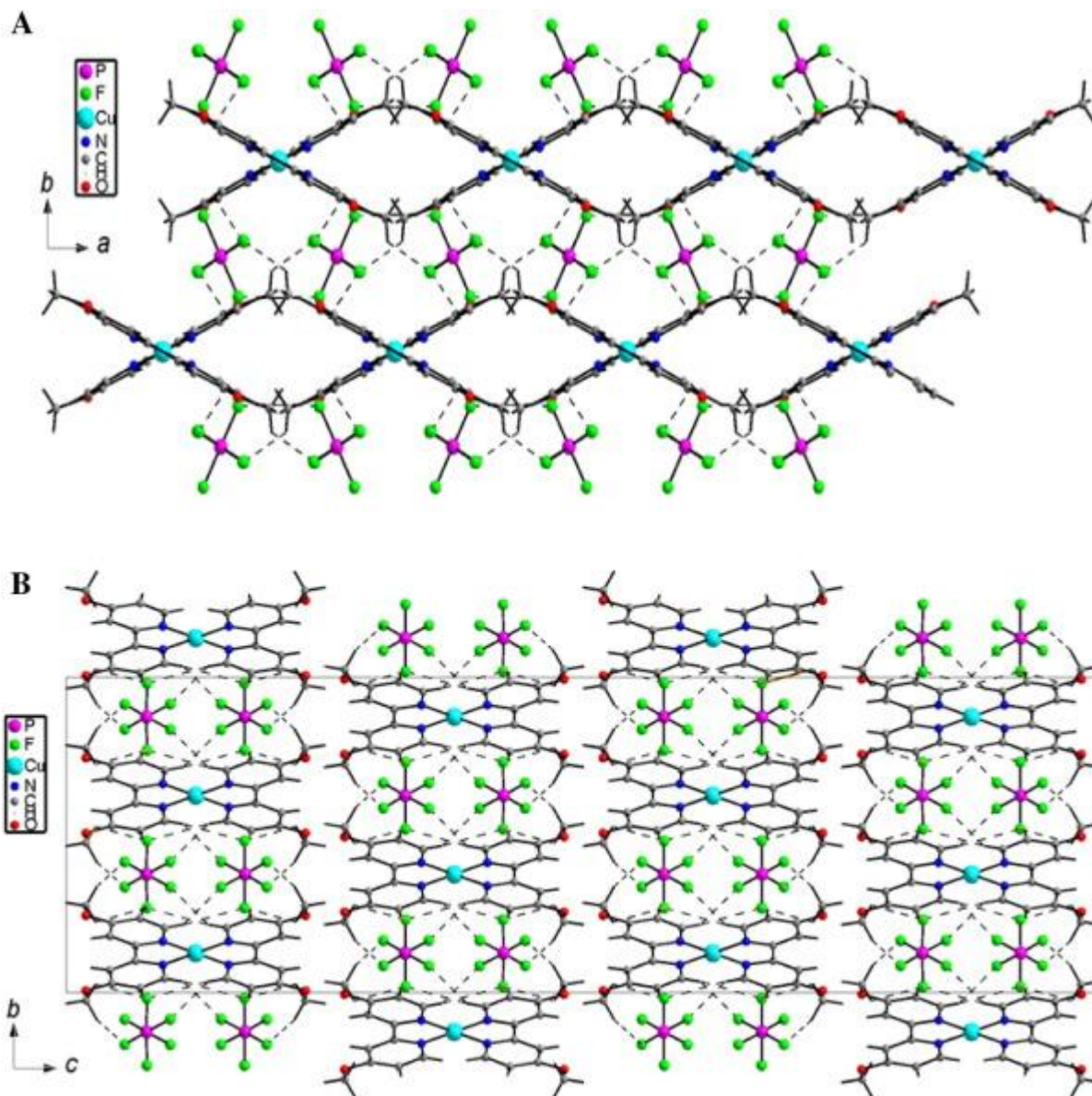


Fig. 2. (A) Pseudo-two-dimensional layer of the complex **1** aligned parallel to the (1 1 0) plane (upper panel) and (B) arrangement of the complex in the unit cell showing the 2D-layers viewed along *a*-axis (lower panel). Dashed lines represent C–H···F weak interactions within the 2D-layer.

3.1.2. Crystal structure of $[\text{Cu}(\text{dimethylbpy})_2\text{Cl}]\text{PF}_6$ (**2**)

The complex **2** was characterized successfully by X-ray diffraction analysis. An ORTEP plot of the complex **2** is shown in Fig. 3. The crystallographic data of the complex are summarized in Table 1. Selected bond lengths and angles are presented in Table 2. The complex **2** consists of discrete mononuclear $[\text{Cu}(\text{dimethylbpy})_2\text{Cl}]^+$ cations and PF_6^- anions. The copper atom is coordinated by four N atoms from two dimethylbpy ligands and one Cl atom in a remarkably distorted geometry

which, for sake of discussion, could be described as trigonal bipyramidal, with the N1, N3 and Cl1 atoms forming the equatorial plane and the N2 and N4 atoms at the vertices. The magnitude of this distortion can be measured by the value of the trigonality index τ ($\tau = (\beta - \alpha)/60$), (β and α are the largest and the second-largest L–M–L angles, respectively, of the coordination sphere; τ is 1 for a perfect trigonal bipyramidal geometry and is zero for a perfect square pyramidal geometry) [40], which for the complex results to be 0.51. The coordination geometry of the complex can be therefore best described as being 51% along the pathway of distortion from square pyramidal to trigonal bipyramidal.

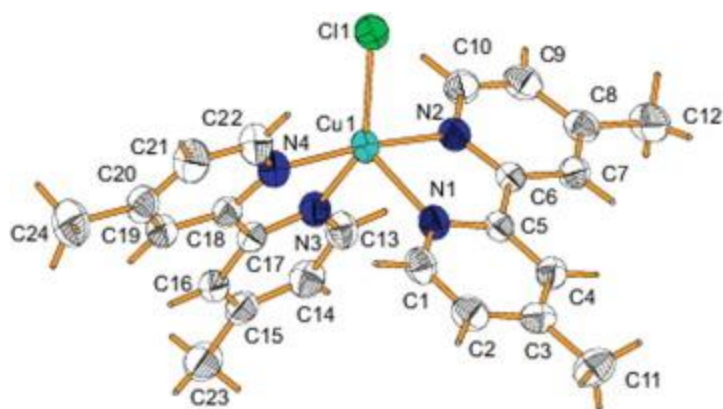


Fig. 3. The molecular structure of the complex **2** with displacement ellipsoids drawn at the 50% probability level. Counter anion (PF_6^-) has been emitted for more clarity. H atoms represent the circle with arbitrary radii.

The bond lengths Cu–N2 and Cu–N4 involving the apical N atoms (mean value 1.991(3) Å) are not significantly different, and are significantly shorter than the two equatorial distances Cu–N1 and Cu–N3 (mean value 2.10(4) Å). The Cu–Cl distance (2.2576(8) Å) is just significantly shorter than those reported previously for the related complexes (2.277–2.350 Å) [41], [42], [43], [44]. The N2–Cu–N4 angle of 173.02(9)° is almost linear, with the N2–Cu–Cl and N4–Cu–Cl angles greater than 90° (91.83(6) and 95.05(7)°, respectively), resulting in the N2 and N4 atoms being bent away from the Cu–Cl bond. There are significant differences in the equatorial angles, which differ from the ideal value of 120° of a regular trigonal bipyramidal stereochemistry (Table 2). The bite angles of the dmbpy ligands are 78.91(8) and 79.51(9)°. In the crystal, the cations are

linked *via* weak $\pi\cdots\pi$ stacking interactions (centroid-to-centroid distances of 3.612(2) and 3.687(2) Å) to form chains running parallel to the *c* axis (Fig. 4).

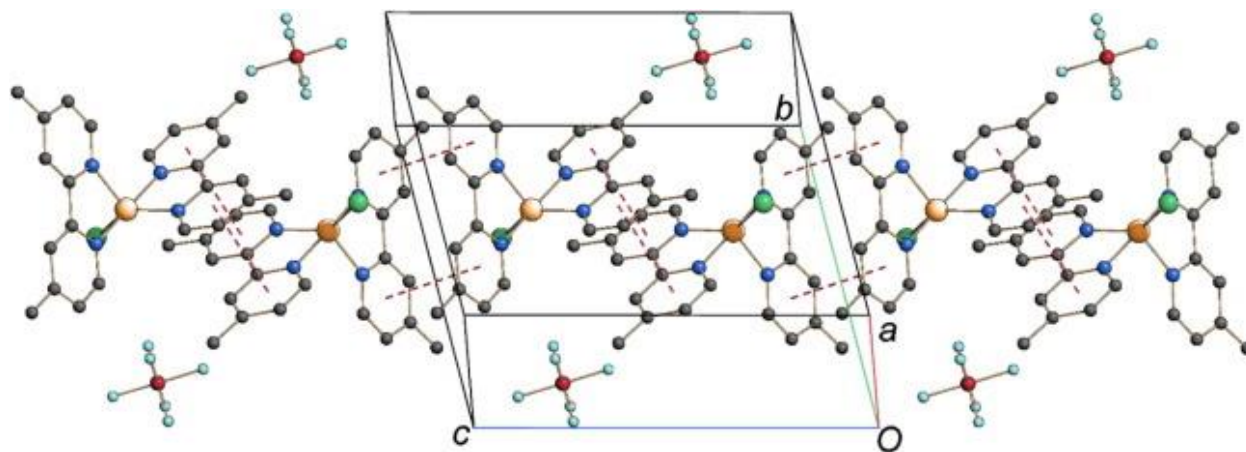


Fig. 4. Crystal packing of the complex **2** showing the formation of a cationic chain through $\pi\cdots\pi$ stacking interactions (red dashed lines) along the *c* axis. Hydrogen atoms are omitted for clarity. (Colour online.)

3.1.3. Hirshfeld surface analysis of $[\text{Cu}(\text{dimethoxybpy})_2](\text{PF}_6)_2$ (**1**) and $[\text{Cu}(\text{dimethylbpy})_2\text{Cl}]\text{PF}_6$ (**2**)

Hirshfeld surface analysis is a recently developed technique which allows insight into all interactions constituting crystal structures [45]. This method uses visual recognition of properties of atom contacts through mapping of a range of functions (d_{norm} , shape index, curvedness, etc.) onto this surface [46]. The increasing popularity of this tool comes from the fact that it allows for recognition of less directional contacts, for instance $\text{C}\cdots\text{H}\cdots\text{F}$ or $\text{H}\cdots\text{H}$ dispersion forces. Another essential advantage is that all (d_i , d_e) contacts created by a molecule of interest can be expressed in the form of a two dimensional plot, known as the 2D fingerprint plot. The d_i and d_e are defined, respectively, as the distance from the Hirshfeld surface to the nearest nucleus outwards from the surface and the distance from the surface to the nearest atom in the molecule itself. The shape of this plot, which is unique for each molecule, is determined by dominating intermolecular contacts [47]. The Hirshfeld surface mapped with a d_{norm} function for the $[\text{Cu}(\text{dimethoxybpy})_2]^{2+}$ and $[\text{Cu}(\text{dimethylbpy})_2\text{Cl}]^+$ cations (Fig. 5) clearly shows the red spots derived from weak $\text{C}\cdots\text{H}\cdots\text{F}$ hydrogen contacts with PF_6^- . The plot of 2D fingerprint for the

[Cu(dimethoxybpy)₂]²⁺ cation (Fig. 5) shows the most significant H···F interactions with contribution of 28.4% and the other interactions H···H (28.2%), C···F (8.8%), O···H (7.8%) and C···H (4.9%). The Hirshfeld surface was calculated using the Crystal Explorer v.3.1 program package and the 2D fingerprint was prepared using the same software [48].

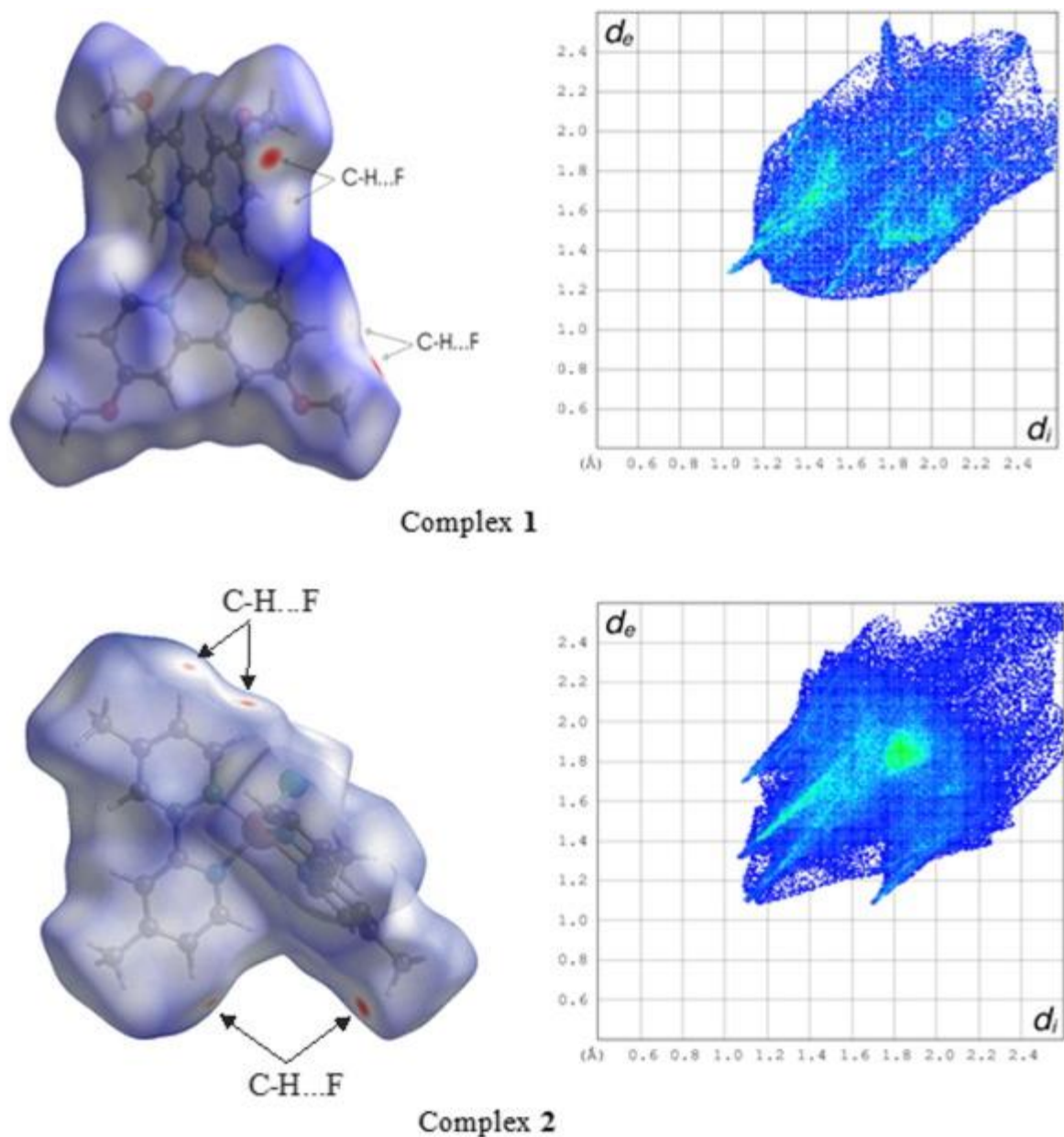


Fig. 5. Hirshfeld surface of **1** and **2** mapped with d_{norm} (red spots indicate close contacts caused by the C-H···F interactions) (left Panels) and the 2D fingerprint (right panels). (Colour online.)

3.2. DNA binding studies

3.2.1. UV–Vis spectral analysis

Absorption titration technique has been used to monitor the binding mode and strength of the interaction between the complexes **1** and **2** with DNA. The UV–Vis absorption spectra of **1** in the absence and presence of DNA is shown in Fig. 6 (for **2** see Supporting Information, Fig. S1). In the absence of DNA, the complex **1** shows characteristic absorption peaks at 231, 276, 285 and 297 nm and the complex **2** shows characteristic absorption peaks at 235, 295 and 306 nm, which are ascribed to the $\pi \rightarrow \pi^*$ electronic transitions of the metal-bound ligands. In general, the hypochromism and red shift are associated with the binding of the complex to the DNA helix, due to the interaction between the aromatic rings of the complex and the base pairs of the DNA [49], [50]. The magnitude of the hypochromism and red shift depends on the strength of the interaction between DNA and the complex. Upon the addition of a solution of DNA to the complexes, a decrease in the absorption intensity (hypochromism) of the $\pi \rightarrow \pi^*$ absorption bands with red shift (2–3 nm) is observed. These spectral characteristics suggest that **1** and **2** interact through a mode that involves a stacking interaction of the planar aromatic rings with the base pairs of DNA with a moderate degree of binding [49], [50]. Furthermore, in order to quantitatively investigate the binding strength of **1** and **2** with DNA, K_b can be obtained by the ratio of the slope to the intercept in the plot of $[\text{DNA}]/(\epsilon_a - \epsilon_f)$ vs. $[\text{DNA}]$, according to the following equation [51]:

$$[\text{DNA}]/(\epsilon_a - \epsilon_f) = [\text{DNA}]/(\epsilon_b - \epsilon_f) + 1/K_b(\epsilon_b - \epsilon_f) \quad (1)$$

in which $[\text{DNA}]$ is the concentration of DNA in base pair, and ϵ_a , ϵ_f and ϵ_b correspond to the apparent absorption coefficient ($A_{\text{obs}}/[\text{complex}]$), the extinction coefficient for the free complex, and the extinction coefficient for the complex in the fully bound form, respectively. The plots of $[\text{DNA}]/(\epsilon_a - \epsilon_f)$ vs. $[\text{DNA}]$ are straight line. The K_b values for **1** and **2** are 0.4×10^4 and $0.1 \times 10^4 \text{ M}^{-1}$, respectively (for **1** see inset plot of Fig. 6 and for **2** see Supporting Information, inset plot of Fig. S1), suggesting that the complex **1** has stronger intercalative binding ability to DNA than the complex **2**. These observed K_b values for the interaction between **1** and **2** with FS-DNA is very smaller than to the value obtained for the typical classical intercalator ethidium bromide (EB; $K_b = 4.94 \times 10^5 \text{ M}^{-1}$) [52] and other the Cu(II) complex with N-donar ligands: $[\text{Cu}(\text{dppt})_2(\text{H}_2\text{O})](\text{PF}_6)_2$; $K_b = 0.86 \times 10^5 \text{ M}^{-1}$) [53], but is similar to the value obtained for other

the Cu(II) complexes with N-donar ligands: ([Cu(phen-dion)(phen)Cl]Cl; $K_b = 0.4 \times 10^4 \text{ M}^{-1}$) and ([Cu(phen-dione)(bpy)Cl]Cl; $K_b = 0.2 \times 10^4 \text{ M}^{-1}$) [54].

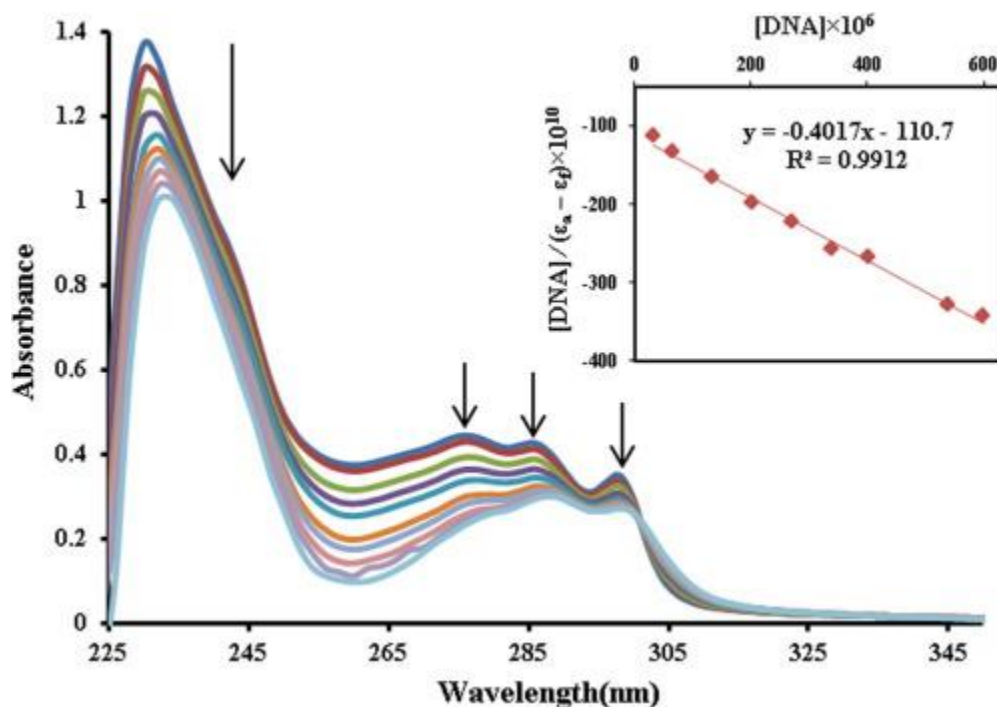


Fig. 6. UV–Vis absorption spectra of the complex **1** ($2 \times 10^{-5} \text{ M}$) with increasing concentrations ($3.4 \times 10^{-5} \text{ M}$ – $60 \times 10^{-5} \text{ M}$) of DNA (Tris buffer, pH = 7.2). The arrows show the absorbance changes upon increasing amounts of DNA. Inset: Plot of $[\text{DNA}]/\epsilon_a - \epsilon_f$ vs. $[\text{DNA}]$.

3.2.2. Fluorescence titration study

Fig. 7 shows the emission spectra of **1** and **2** in the absence and presence of increasing amounts of DNA at 310 K at $\lambda_{\text{ex}} = 270 \text{ nm}$ (for 290 and 300 K see Supporting Information, Fig. S2). In the absence of the DNA, the complexes are emissive (for **1** and **2** λ_{em} is 312 and 320 nm, respectively). As shown in Fig. 7, addition of DNA led to the decrease in the emission intensities of **1** and **2**, without any significant shift in the position of the maximum emission wavelength. The results indicate that an interaction between the complexes **1** and **2** with DNA has occurred. The quenching constant (K_{SV}) is a quantitative estimate of quenching behavior and can be obtained by analyzed the data according to the linear Stern–Volmer (Eq. (2)) [55]:

$$I_0/I = 1 + K_{\text{SV}}[Q] \quad (2)$$

in which I_0 and I are the emission intensities in the absence and presence of the quencher, respectively. $[Q]$ is the concentration of [DNA] and K_{SV} is the Stern–Volmer quenching constant, which is a measure of the efficiency of fluorescence quenching by DNA. Fig. S3 indicates plots of I_0/I vs. [DNA] at three different temperatures. The plots of I_0/I vs. [DNA] are linear within the experimental concentration range. This suggests that only a single type of quenching exists in the complex–DNA interaction [56]. Table 3 shows the calculated values of K_{SV} for the interaction of **1** and **2** with DNA at different temperatures. As seen in Table 3, the calculated K_{SV} values increases with rising temperature. This increasing of K_{SV} values with increasing temperatures indicates that the quenching mechanism of binding reaction between the complexes **1** and **2** with DNA is dynamic quenching [56].

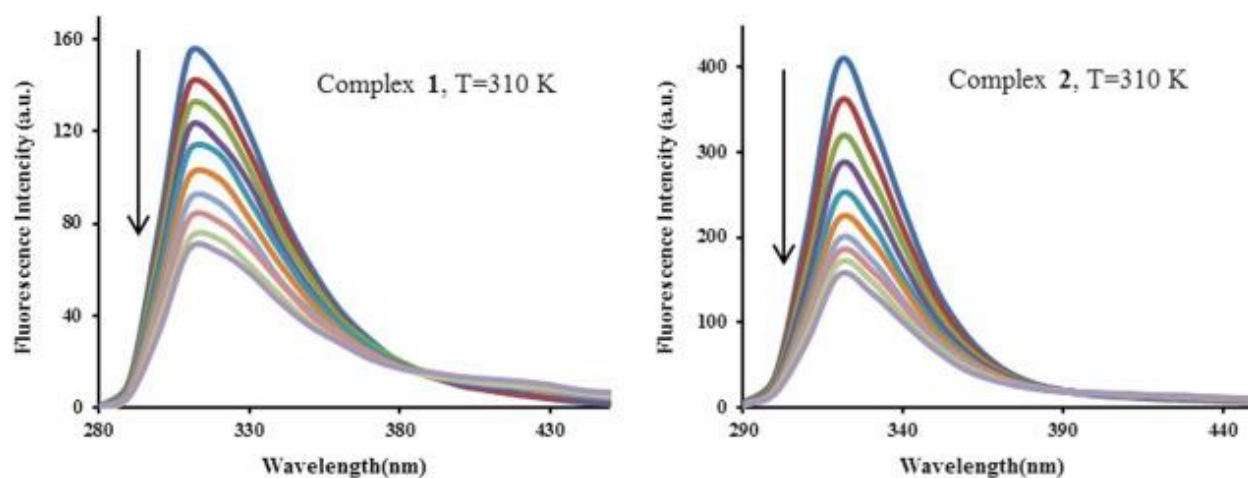


Fig. 7. Emission spectra of the complexes **1** and **2** (4.0×10^{-5} M) with increasing concentrations (3.0×10^{-5} M– 27×10^{-5} M) of DNA (Tris buffer, pH = 7.2) at 310 K. The arrows show the emission intensity changes upon increasing amounts of DNA.

Table 3. K_{SV} , K_{bin} and n values for the complex–DNA systems at three different temperatures.

Complex	T (K)	K_{SV} ($\times 10^4$ M $^{-1}$)	R^2	K_{bin} ($\times 10^5$ M $^{-1}$)	n	R^2
1	290	0.33	0.9934	0.39	1.3	0.9907

Complex	T (K)	K_{SV} ($\times 10^4 M^{-1}$)	R^2	K_{bin} ($\times 10^5 M^{-1}$)	n	R^2
2	300	0.40	0.9901	0.50	1.3	0.9933
	310	0.50	0.9926	0.66	1.3	0.9978
	290	0.45	0.99	1.2	1.4	0.9904
	300	0.51	0.9907	1.9	1.4	0.9963
	310	0.64	0.9988	3.6	1.5	0.9928

To have a better understanding of the type of the non-covalent interaction between DNA and the complexes **1** and **2**, the sign and magnitude of the thermodynamic parameters, enthalpy change (ΔH°) and entropy change (ΔS°), are the main factors [57]. Parameters ΔH° and ΔS° Can be obtained from van't Hoff (Eq. (3)):

$$\log K_{bin} = -\frac{\Delta H^\circ}{2.303 RT} + \frac{\Delta S^\circ}{2.303 R} \quad (3)$$

where, K_{bin} is the binding constant, T is the absolute temperature in K, and R is the gas constant. ΔG° Can be evaluated using Eq. (4):

$$\Delta G^\circ = \Delta H^\circ - T\Delta S^\circ = -RT \ln K_{bin} \quad (4)$$

The binding constant (K_{bin}) in Eq. (3) can be obtained using the double-logarithm Eq. (5):

$$\log[(I_0 - I)/I] = \log K_{bin} + n \log[Q] \quad (5)$$

in which K_{bin} is the binding constant for the interaction of the Cu(II) complexes with DNA and n is the number of the binding sites on the DNA molecule.

Fig. S4 displays the plots of $\log [(I_0 - I)/I]$ vs. $\log [DNA]$ at three different temperatures and the values of K_{bin} and n can be determined from the intercept and slope of this plots, respectively. As seen in Fig. S5, the van't Hoff plots of $\log K_{bin}$ vs. $1/T$ give straight line. Table 3 shows the calculated K_{bin} and n values at three different temperatures for DNA-complex system. It has been found that the magnitude of the binding constants increase with increasing temperature, which

shows the binding process, is endothermic. The calculated values of n are around one for the complexes indicating the existence of a single binding site in DNA for the complexes. Table 4 indicates the values of ΔG° , ΔH° and ΔS° for the interaction of the complexes with DNA. The negative values of ΔG° demonstrate that the binding process is always spontaneous. The positive values of ΔH° and ΔS° have been calculated for complex–DNA interaction. Here $T\Delta S^\circ$ is greater than ΔH° which indicates that the binding of the complexes with DNA is entropy driven reaction. The positive values of ΔH° and ΔS° indicate that the hydrophobic interactions play a major role in the binding of the complexes to DNA [57]. Thus, the higher emission quenching propensity of **2** by DNA could be due to better hydrophobic nature of **2** than **1**. The changes of ΔG° values (Table 4) indicate that the spontaneity of complex–DNA binding reaction increases with increasing the temperature from 290 to 310 K.

Table 4. Thermodynamic parameters for the complex–DNA system at three different temperatures.

Complex	T (K)	ΔG° (kJ mol ⁻¹)	ΔH° (kJ mol ⁻¹)	ΔS° (J mol ⁻¹ K ⁻¹)	R^2
1	290	-25.3	+21.1	+160	0.9973
	300	-26.9			
	310	-28.5			
2	290	-27.6	+44.0	+247	0.9944
	300	-30.1			
	310	-32.5			

3.2.3. Viscosity measurements

In order to understand the nature and mode of DNA binding of the complexes, viscosity measurements were carried out. The values of the relative specific viscosity $(\eta/\eta_0)^{1/3}$, where η and η_0 are the specific viscosities of DNA in the presence and absence of the complex, are plotted against R ($=[\text{complex}]/[\text{DNA}]$, Fig. S6). When small molecules intercalate between the

neighboring base pairs of DNA, the double helix loosens to accommodate the molecule, which increases the length of the DNA helix. Since the viscosity of DNA solution is very sensitive to the changes of DNA length, the increased viscosity of DNA solution can be associated with the specific intercalation. A classical DNA intercalator like ethidium bromide shows a significant increase in the viscosity of the DNA solutions. In contrast, a partial and/or non-intercalation of the complex could result in less pronounced effect on the viscosity [58]. The increase in the viscosity observed for the complex **1** is higher than that for the complex **2**, but both is less than that for the potential intercalator EB [9]. The partial insertion of **1** in between the DNA base pairs is deeper than that of **2** [58].

3.2.4. Competitive DNA-binding studies

The binding abilities of the complexes to DNA were investigated by competitive binding in which they served as an intercalative binding probe in competition with GelRed. GelRed is a stable, sensitive and environmentally safe fluorescent nucleic acid dye introduced by Biotium to replace the highly toxic ethidium bromide in gel electrophoresis and other experimental techniques [59], [60]. GelRed is structurally closely related to ethidium bromide and consists of two ethidium subunits that are linked by a linear spacer [59], [61]. When GelRed bound to DNA, absorption and emission spectra are essentially identical to those of ethidium bromide according to its manufacturer (Biotium, Hayward, CA, USA). We can directly replace EB with GelRed for the advantage of being much less toxic and mutagenic, because the chemical structure of the dye was designed such that the dye is incapable of crossing cell membranes [59]. Both GR and EB inserting themselves between the base pairs in the double helix and forms soluble complexes with nucleic acids, therefore their fluorescence intensity increases in the presence of DNA [61], [62]. Furthermore, both GR and EB bound with DNA emit characteristic fluorescence at around 597 nm when excite at 520 nm [61], [62]. The competitive binding studies involve the addition of **1** and **2** to DNA incubated with GR ([DNA]/[GR] = 10:1) and then the measurement of the emission intensities of GR-DNA system. Fig. 8 shows the emission spectrum of the GR-DNA solution in the absence and presence of **1** and **2**. The emission intensity of GR–DNA system at 597 nm significantly decreased when the concentration of the complexes increased. The % fluorescence decrease is directly related to the extent of DNA binding, providing relative binding affinities [63]. The quenching of the initial GR–DNA fluorescence is 85% for the complex **1** and

68% for the complex 2 ($[I_0 - I/I_0] \times 100$), which reveals that the complex 1 has stronger binding affinity to DNA than the complex 2. The quenching constants (K_{SV}) can be obtained by analyzed the data according to the linear Stern–Volmer (Eq. (2)). The plots of I_0/I vs. $[\text{complex}]/[\text{DNA}]$ are linear lines (Fig. 8 inset) and K_{SV} values were calculated by the slope of these plots. The K_{SV} value for the complex 1 is 17.8 M^{-1} while that for the complex 2 is 5.7 M^{-1} , which reveals that complex 1 has higher ability of replacing GR from DNA–GR system DNA than the complex 2. The results suggest that the complexes can compete for DNA-binding sites with GR and displace GR from the DNA–GR system, which is usually characteristic of the intercalative interaction of compounds with DNA [63].

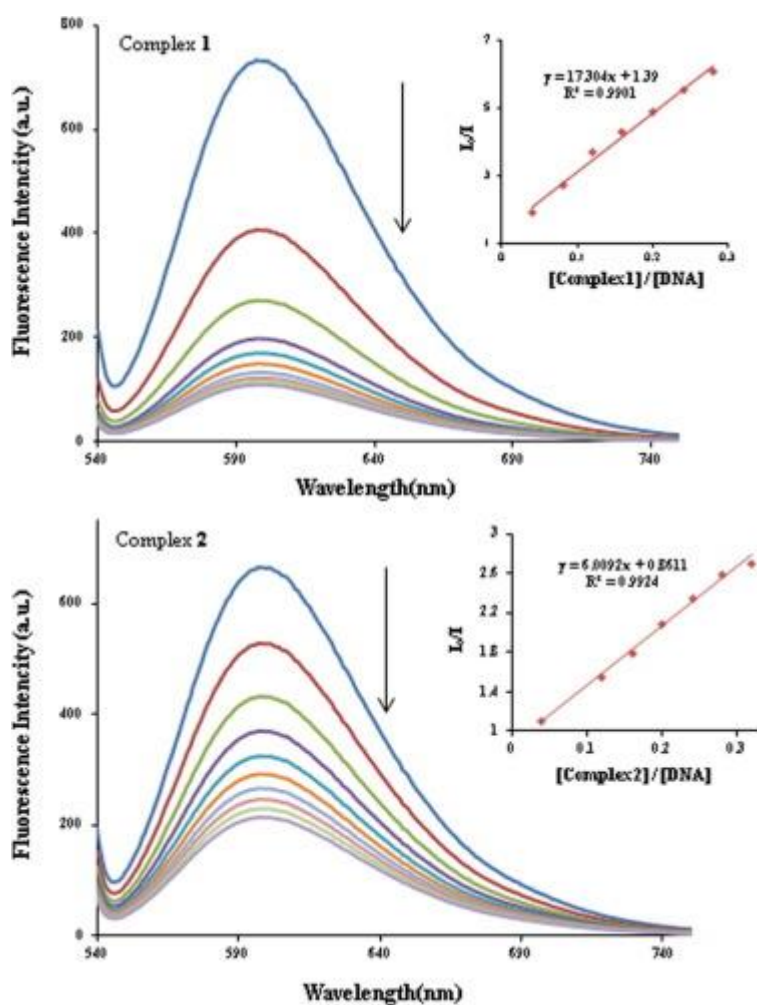


Fig. 8. Emission spectra of GR-DNA in the absence and presence of the complexes 1 and 2 in Tris/NaCl buffer (pH = 7.2). $[\text{GR}] = 1 \times 10^{-5} \text{ M}$, $[\text{DNA}] = 1 \times 10^{-4} \text{ M}$ and $[\text{complex}] = (0.0, 4.0,$

8.0, 12, 16, 20, 24, 28, 32, and 36) $\times 10^{-6}$ M. The arrows indicate the emission intensity changes upon increasing the concentration of the complexes. Inset: The plots of I_0/I vs. [complex]/[DNA].

3.2.5. Circular dichroism spectral analysis

Circular dichroism (CD) is a useful technique which may give us useful information on how the conformation of the DNA chain is influenced by the bound complex. The CD spectrum of DNA consists of a positive band at 277 nm due to the π - π base stacking of DNA and a negative band at 247 nm due to helicity, which is also characteristic of DNA in a right-handed B form [64]. The CD spectrum of DNA is very sensitive to its conformational changes. It is generally accepted that covalent and intercalative binding can influence the tertiary structure of DNA and induce changes in the CD spectra of DNA, while external binding modes (electrostatic interaction or groove binding) show less or no perturbation on the base-stacking and helicity bands [65]. The CD spectra of DNA were monitored in the presence of **1** and **2**. As shown in Fig. 9, the intensities of both bands decrease while no considerable shift in their positions appears as the complexes are added to the solution of DNA. It may be a consequence of the intercalation interaction inducing conversion from a more B-like to a more C-like structure within the DNA molecule [66]. An isobestic point, well defined for the all titration course, shows the presence of two DNA absorbing species, the free and the bound to the copper complexes.

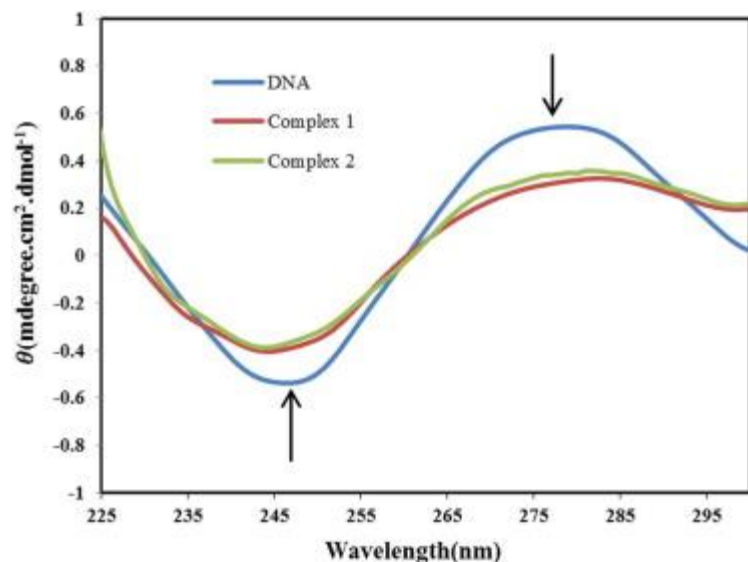


Fig. 9. Circular dichroism spectra of DNA bound by the complexes **1** and **2**, [DNA] = 5×10^{-5} M and [complex] = 1×10^{-6} M.

3.2.6. Electrochemical study

The application of electrochemical methods to the study of coordination of metal ions and chelates to DNA provides a useful complement to the previously used methods of investigation. The Cu(II) complexes generally have sensitive electrochemical signal because of the strong and easy electron donation-acceptance properties between Cu^+ and Cu^{2+} . Fig. 10 shows CV behavior of the complex **1** (3.0×10^{-4} M) in the absence and presence of DNA in 1:10 DMSO-buffer solution (5 mM Tris/10 mM NaCl) in the range of +0.3 to -0.55 V with a scan rate of 100 mV/s (for **2** see Supporting Information, Fig. S7). Summaries of voltammetric results are given in Tables 5. The net shift in the formal potential, $E^{o'}$ or voltammetric $E_{1/2}$ (the average of E_{pc} and E_{pa}), on addition of DNA can be used to estimate the ratio of equilibrium constants for the binding of Cu^{2+} and Cu^+ ions to DNA (K_{2+}/K_+) by using Scheme S1 in Supplementary material and the Nernst equation:

$$E_b^{o'} - E_f^{o'} = 0.0591 \log(K_+/K_{2+}) \quad (6)$$

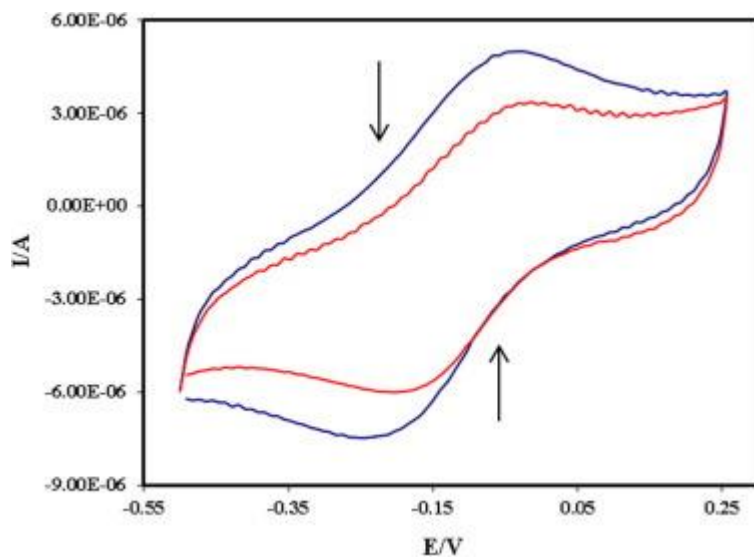


Fig. 10. Cyclic voltammograms of the complex **1** in the absence and presence of DNA in Tris buffer, pH = 7.2 (scan rate 100 mV/s). [complex] = 30×10^{-5} M and [DNA] = 10×10^{-5} M.

Table 5. Voltammetric behavior of **1** and **2** in the absence and presence of DNA.

Compound	E_{pc}/V	E_{pa}/V	I_{pc}/A	I_{pa}/A	$E_{1/2}/V$
1	-0.24	-0.04	-7.5×10^{-6}	5.0×10^{-6}	-0.14
1 + DNA	-0.2	-0.02	-6.0×10^{-6}	3.3×10^{-6}	-0.11
2	-0.18	-0.04	-2.7×10^{-6}	6.0×10^{-7}	-0.12
2 + DNA	-0.16	-0.05	-2.0×10^{-6}	4.0×10^{-7}	-0.10

According to the literature [67], if the interaction mode is an electrostatic binding nature, the formal potential shifts to a more negative value, while intercalative binding results in a formal potential shift to a more positive value. Results of CV show a positive shift in $E^{o'}$ ($K_+/K_{2+} > 1$). Thus, according to the above results, two complexes interact with DNA by intercalative binding mode. The current intensity of cathodic and anodic peaks decreased significantly, suggesting the existence of an interaction between the complexes and DNA. The reduction in the peak currents due to slow diffusion of an equilibrium mixture of the free and DNA bound complex to the electrode surface [67].

3.3. BSA binding studies

3.3.1. UV-Vis absorption studies

BSA has two main absorption bands including: (i) one weak band at the wavelength range near 280 nm, where only the aromatic side chains of the protein absorb, (ii) one strong band at the wavelength range near 210–230 nm, where, in addition to the aromatic amino acids, histidine, cystine, and the peptide group all contribute to the absorption [68]. Fig. 11, Fig. 12 shows the absorption spectra of the solution of BSA upon addition of increasing amounts of **1** and **2**, respectively at wavelength of around 200–320 nm. Upon addition of **1** and **2** to the BSA solution, the intensity of the absorption peak of BSA at 230 nm obviously decreased, and the peak shifted toward longer wavelength (with 70% hypochromicity and 4 nm red shift for the complex **1** and 31% hypochromicity and 4 nm red shift for the complex **2**). While the intensity of the peak of BSA at 278 nm decreases upon addition of **1** to the BSA solution and increases upon

addition of **2**. These observations (hypochromic effect and red shift) indicate that there is the strong interaction between **1** and **2** with aromatic amino acids of BSA, that may cause the conformational changes in BSA and change the polarity of the microenvironment around amino acids of BSA [68], [69]. The results show the complex **1** has stronger binding ability to BSA than the complex **2**.

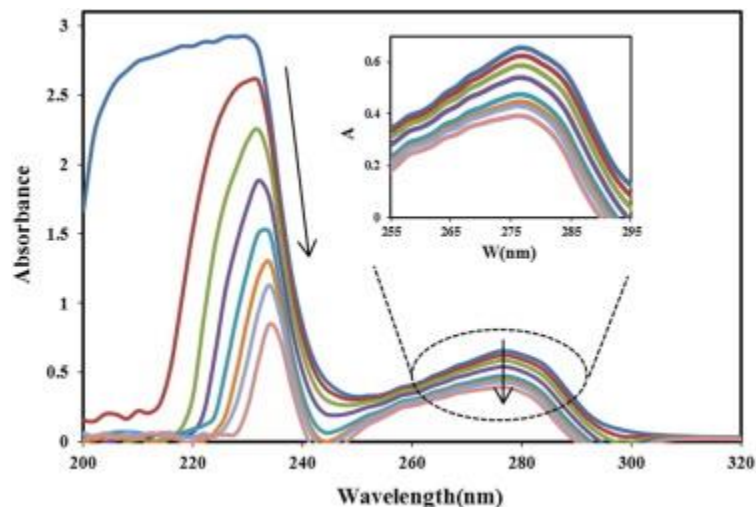


Fig. 11. UV-Vis absorption spectra of BSA (15×10^{-6} M) with increasing concentrations (2×10^{-6} M– 14×10^{-6} M) of the complex **1** (Tris buffer, pH = 7.2). The arrows show the absorbance changes upon increasing amounts of the complex.

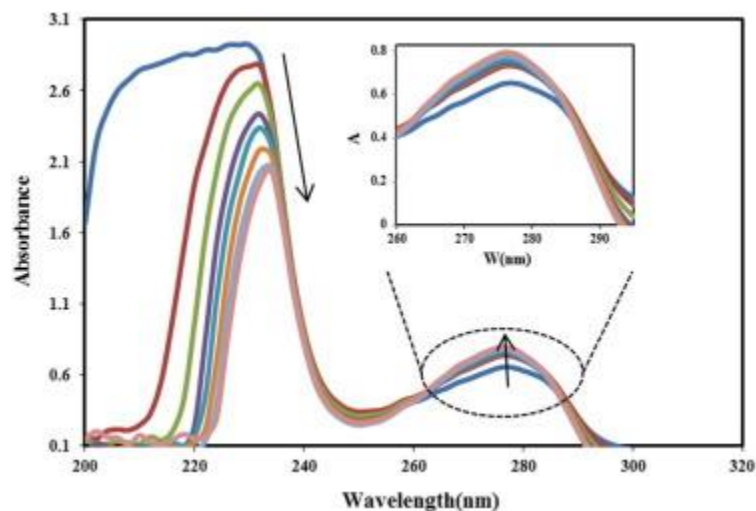


Fig. 12. UV–Vis absorption spectra of BSA (15×10^{-6} M) with increasing concentrations (2×10^{-6} M– 14×10^{-6} M) of the complex **2** (Tris buffer, pH = 7.2). The arrows show the absorbance changes upon increasing amounts of the complex.

3.3.2. Fluorescence quenching studies

Fig. 13 displays the emission spectra of BSA in the absence and presence of **1** and **2** at $\lambda_{\text{ex}} = 280$ nm. It should be noted that in conditions of this experiment the emission spectrum of the Cu(II) complexes has the lowest intensity (almost zero), which suggests that the effect of the complexes would be negligible. Addition of the complexes **1** and **2** to BSA led to a decrease in the fluorescence intensities of BSA at 344 nm. The quenching provoked by the complexes (Fig. 13) is significant (up to 48% of the initial fluorescence intensity for **1** and 53% for **2**). The changes in the emission spectra of BSA are primarily due to change in protein conformation, subunit association, substrate binding, or denaturation [70]. These results clearly indicate the binding of each complex to BSA, which quenches the intrinsic fluorescence of BSA. The quenching constants (K_{SV}) can be obtained by analyzed the data according to the linear Stern–Volmer (Eq. (2)) [55]. The plots of I_0/I vs. [complex]/[BSA] are linear lines (Fig. 13 inset) and K_{SV} values were calculated by the slope of these plots. The K_{SV} value for the complex **1** is 1.0 M^{-1} while that for the complex **2** is 1.5 M^{-1} . The higher BSA emission quenching propensity of **2** could be due to better hydrophobic nature of **2** than **1**.

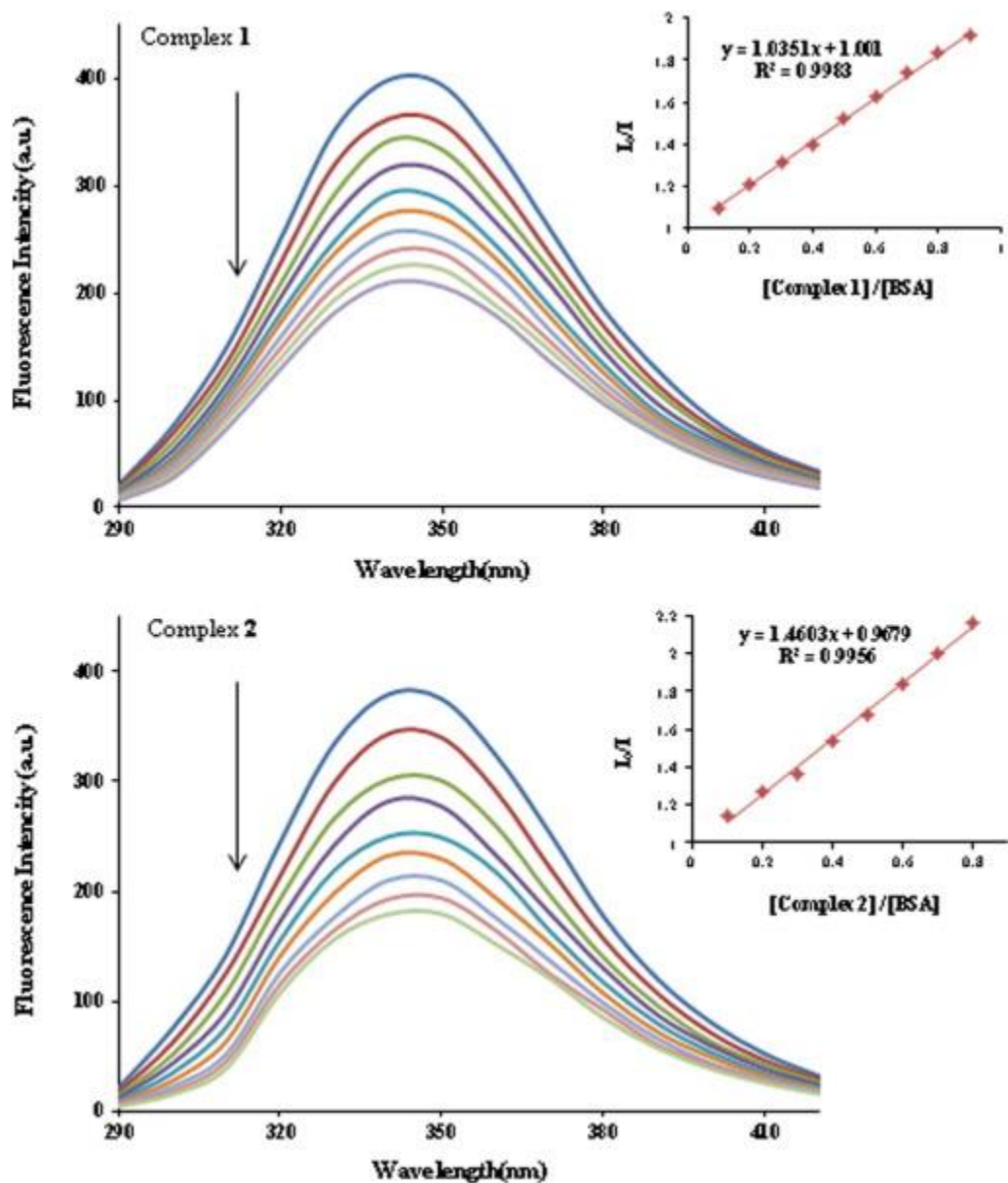


Fig. 13. Emission spectra of BSA (4×10^{-6} M) in the absence and presence of the complexes 1 and 2 with increasing [complex]/[BSA] ratios range from 1:1 to 8:1 (Tris buffer, pH = 7.2). The arrows show the emission intensity changes upon increasing amounts of the complexes.

3.3.3. Characteristics of synchronous fluorescence spectra

In order to study the structural changes of BSA in the presence of the complexes, changes in synchronous fluorescence spectra of BSA were measured. In synchronous fluorescence spectra of

BSA, when the $\Delta\lambda$ value is 15 nm, the synchronous fluorescence is characteristic of tyrosine residue whereas a larger $\Delta\lambda$ value of 60 nm is characteristic of tryptophan [71]. Fig. S8 shows the effect of increasing the concentration of **1** and **2** on the synchronous spectra of BSA at $\Delta\lambda = 15$ and 60 nm. When the concentration of the complexes increased, the fluorescence intensity of the tyrosine and tryptophan ($\Delta\lambda = 15$ and $\Delta\lambda = 60$ nm) decrease. The results show that the interaction of **1** and **2** with BSA affects the conformation of both the tryptophan and tyrosine micro-regions. The synchronous measurements confirmed the effective binding of the complexes with the BSA [71].

3.3.4. Circular dichroism studies

To explore the conformational effects on the protein secondary structure, CD measurements of the BSA solution at room temperature have been carried out in the presence of **1** and **2**. Samples were prepared at [BSA]/[complex] ratio (1:1) and analyzed through circular dichroism spectroscopy in the range of 200–260 nm. In the UV region of the CD spectrum of BSA, two strong negative bands, at 210 nm and 224 nm, are present as typically observed in proteins with a high amount of α -helical secondary structure, and are related to the $n \rightarrow \pi^*$, $\pi \rightarrow \pi^*$ transitions associated with the peptide bond [72]. By interacting with serum proteins, metal complexes induce conformational changes of the protein molecule, differing in the degree of structural distortion [73]. The spectra unequivocally show the changes in the secondary structure of the BSA caused by two complexes (Fig. 14). In the case of the complex **1**, there is a significant change on the CD spectrum of the protein, the CD intensity of BSA significantly decreased (shifting to zero levels) and the peak shifted toward longer wavelength. While the CD intensity of BSA decrease (shifting to zero levels) without any significant shift of the peaks with increasing the complex **2** to BSA. In agreement with the previous results, the conformational changes of the protein molecule induced by the complexes **1** and **2** are evident, and they bear out potential secondary interactions (electrostatic and/or steric) between the protein and the copper(II) complexes, which can allow the BSA to play an important role in both the stabilization and the transport of Cu(II) in the body.

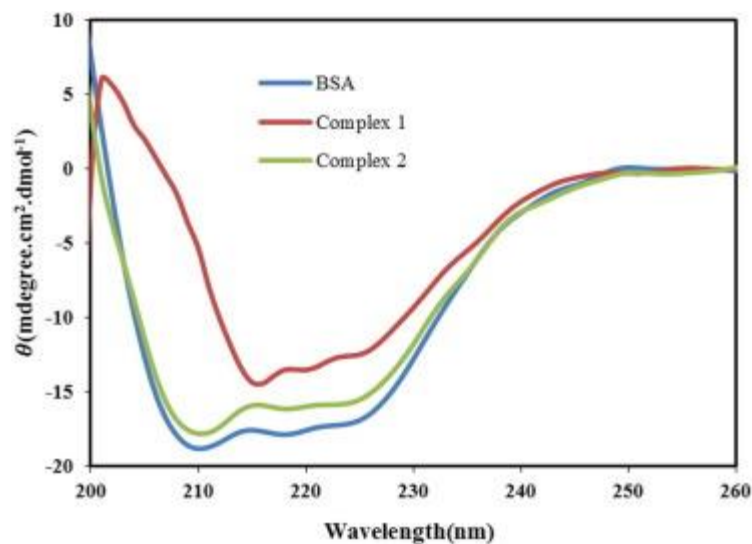


Fig. 14. CD spectra of the BSA–complex system at 298 K. $[BSA] = 2 \times 10^{-6}$ M and $[complex] = 2 \times 10^{-6}$ M.

3.4. Molecular docking

3.4.1. Molecular docking of the Cu(II) complexes with DNA sequence $d(ACCGACGTCGGT)_2$

The obtained results from docking of the complexes to DNA sequence $d(ACCGACGTCGGT)_2$ reveal that the Cu(II) complexes fitted into the DNA minor groove (Fig. 15). The binding energy value for the complex 1 is -6.12 and for the complex 2 is -5.95 kcal mol⁻¹, which reveals that the complex 1 has stronger binding affinity to DNA than the complex 2. As seen in Table 6, there are five categories of hydrophobic contacts between the complex 1 and bases of DNA, including, DG 7, DC 9, DG 10, DC 18 and DT 20. Also, the complex 1 is able to form two hydrogen bonding interactions with DA 17 and DG 19. While, there are seven categories of hydrophobic contacts between the complex 2 and bases of DNA, including, DT 8, DC 9, DG 10, DG 16, DA 17, DC 18 and DG 19. Thus, hydrophobic and hydrogen bonding interactions play significant role in stabilizing of the complex 1 and just hydrophobic interactions in stabilizing of the complex 2 in minor groove of DNA.

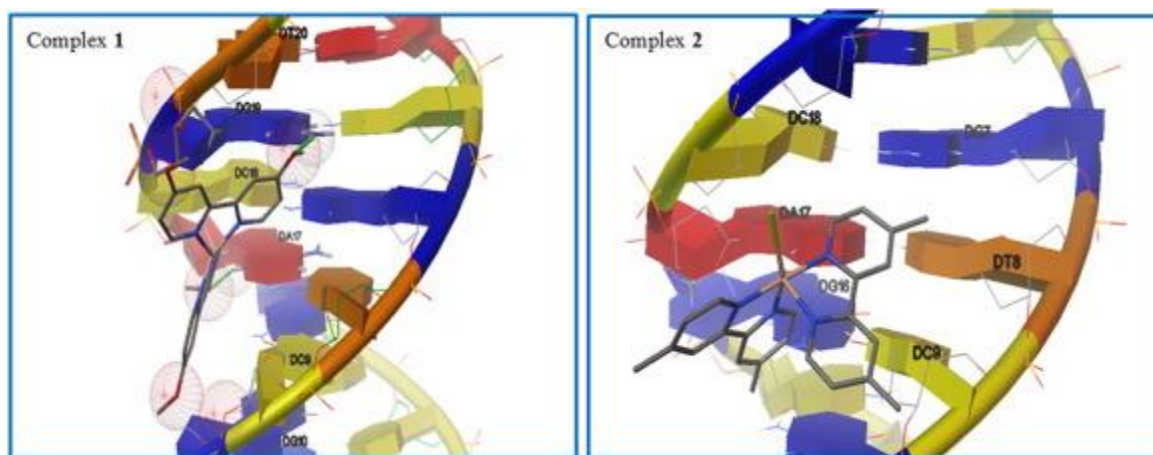
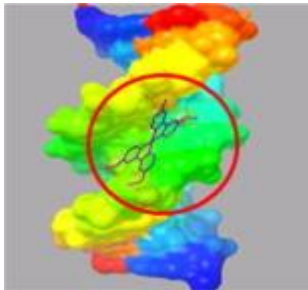
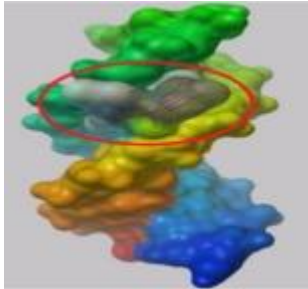


Fig. 15. The docked Cu(II) complexes in the minor groove of DNA sequence d(ACCGACGTCGGT)₂, (for the complex 1, the red spheres represent H-bond interactions). (Colour online.)

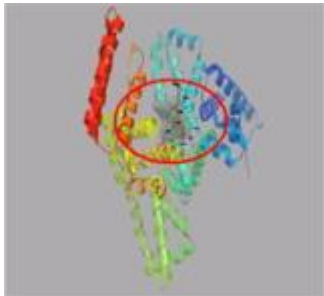
Table 6. The results of molecular docking of Cu(II) complexes to DNA.

Compound	Binding site	Type of interactions	of Adjacent nucleotides within 3 Å distances to complex
1		H-bond hydrophobic	and DG 7, DC 9, DG 10, DA 17, DC 18, DG 19, DT 20
2		Hydrophobic	DG10, DC9, DG16, DA17, DT8, DC18, DG7, DG19

3.4.2. Molecular docking of the Cu(II) complexes with BSA

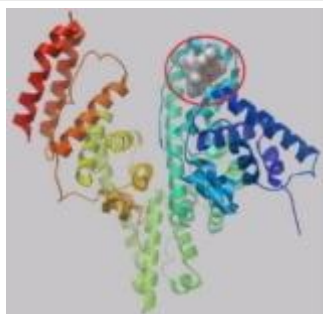
It has been confirmed that the binding affinity of drugs to serum albumin is the major factor affecting on the distribution and the metabolism of drugs. Therefore the study of interaction between serum albumin and drug is essential to investigate the pharmacokinetics and availability of drugs in tissues. Serum albumin as the most abundant carrier protein comprises three α -helical domains (I, II and III). Table 7 shows the best energy-ranked result of the interaction between the Cu(II) complexes and BSA in all runs of docking procedure. The obtained results from molecular docking show that **1** and **2** are suited within the domain I with the binding energy of -7.54 and $-8.00 \text{ kcal.mol}^{-1}$, respectively (Fig. 16). The complex **1** is nearby to some hydrophobic residues in domain I of BSA (Leu 112, Leu 189, Ala 193 and Tyr 147). Some of the residues in the neighborhood of the complex **1** (Asp 108, Ser 109, Pro 110, Asp 111, His 145, Pro 146, Arg 196 and Asn 457) are polar. Also, the complex is able to form a π -cation interaction with Arg 458 and a hydrogen bonding interaction with Leu 454, thus these residues play significant role in stabilizing of the complex **1** interaction. On the other hand, there are hydrophobic contacts between the complex **2** with some hydrophobic residues in domain I of BSA (Leu 122, Phe 133 and Pro 117). Some of the residues in the neighborhood of the complex **2** (Thr 121, Glu 125, Glu 140, Lys 136 and Tyr 137) are polar. Also, there is a π -cation interaction between the complex **2** with Lys 136, thus these residues play significant role in stabilizing of the complex **2** interaction (Fig. 16).

Table 7. The results of molecular docking of Cu(II) complexes to BSA.

Compound	Binding site	Type of interactions	of Adjacent amino acids within 3 Å distances to complex
1		π -Cation, H-bond and hydrophobic	Asp 108, Ser 109, Pro 110, Asp 111, Leu 112, His145, Pro 146, Tyr 147, Leu 189, Ala 193, Arg 196, Leu 454, Asn 457, Arg 458

Compound	Binding site	Type of interactions	of Adjacent amino acids within 3 Å distances to complex
----------	--------------	----------------------	---

2



π -Cation and hydrophobic interactions with Leu 122, Phe 133, Thr 121, Pro 117, Glu 125, Lys 136, Glu 140, Tyr 137

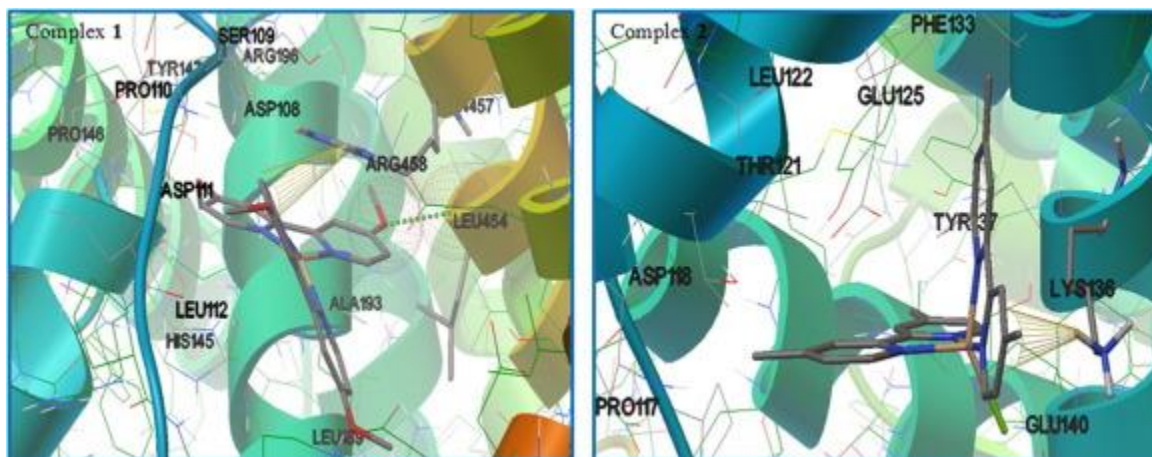


Fig.

16. The docked Cu(II) complexes in the domain I of BSA (the yellow cones and red spheres represent π -cation and H-bond interactions, respectively). (Colour online.)

3.5. *In vitro* cytotoxicity studies

The cytotoxicity of the DNA binding complexes **1** and **2** on MCF-7, A-549 and HT-29 human cancer cell lines has been evaluated by using MTT assay. Fig. 17, Fig. 18, Fig. 19 show live cells images at magnification of 320X, which were acquired directly using an inverted microscope without any treatment or staining. Microscopic analyses of the cancer cells treated with **1** and **2** show the morphological changes in the cancer cells with increasing the concentration of the complexes. Fig. 20 shows plots of percentage of viability vs. concentration of the complexes **1** and **2**. Table 8 shows the IC_{50} values obtained from MTT assay for the complexes **1** and **2** and cisplatin as a reference metallodrug. Based on the results obtained from

MTT assay, it would appear that the complex **2** exhibit better cytotoxicity than the complex **1** and cisplatin under the same experimental conditions. This clearly indicates that the anticancer activity of the complexes is varies with the extent of their interaction with DNA. While **1** exhibits high cytotoxic effects, but the complex **2** is remarkable in displaying a cytotoxic effect. It is evident that the hydrophobic forces of interaction of the methyl groups on the 4 and 4' positions of the bipyridine ring in the complex **2** lead to its highest cytotoxicity. These observations are similar to the obtained results that previously reported for other complexes [9]. These results reveal that the tested cancer cells are more sensitive to the complex **1** than cisplatin. Also results show that the complex **2** exhibits better cytotoxicity against A-549 cell line than other cell lines under the same experimental conditions, especially in 1 μM concentration. For the complex **2** no further cell inhibition against cell lines was observed upon treatment higher than 20 μM .

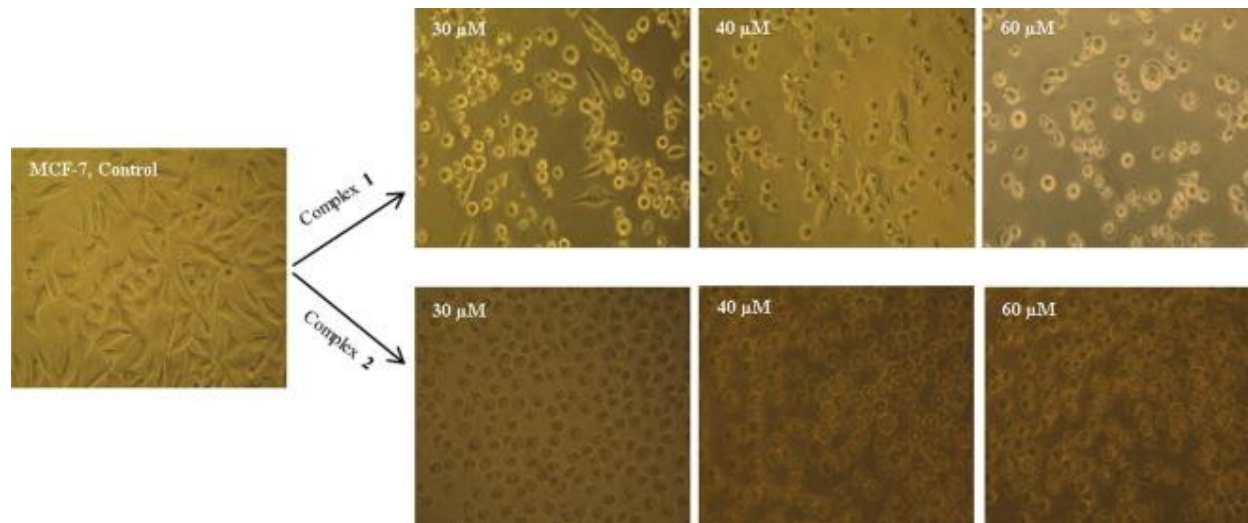


Fig. 17. The microscopic images of MCF-7 cancer cells treated with the Cu(II) complexes at magnifications of 320 \times .

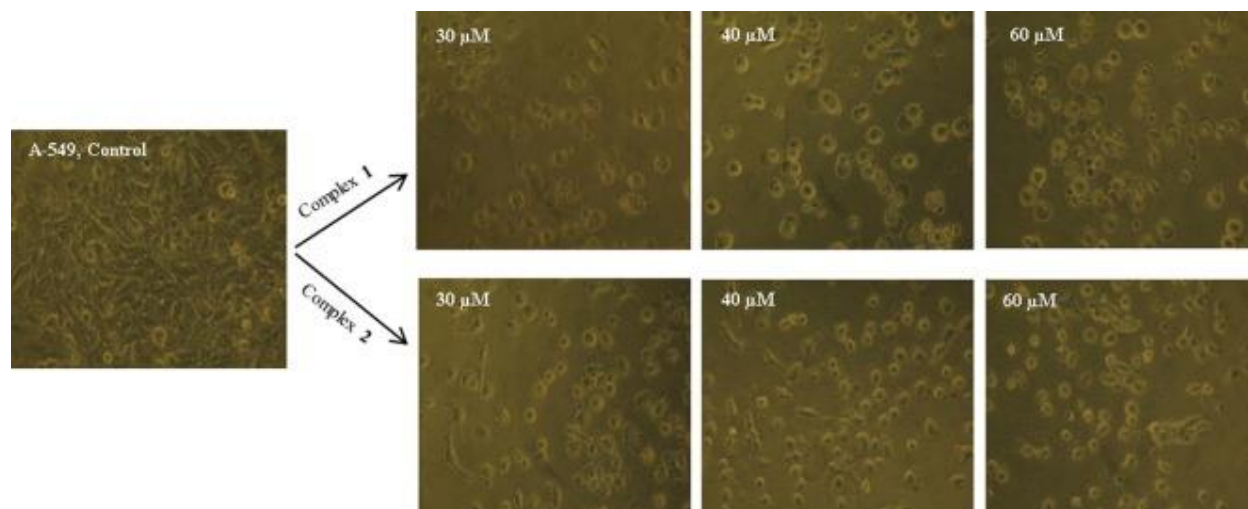


Fig. 18. The microscopic images of A-549 cancer cells treated with the Cu(II) complexes at magnifications of 320 \times .

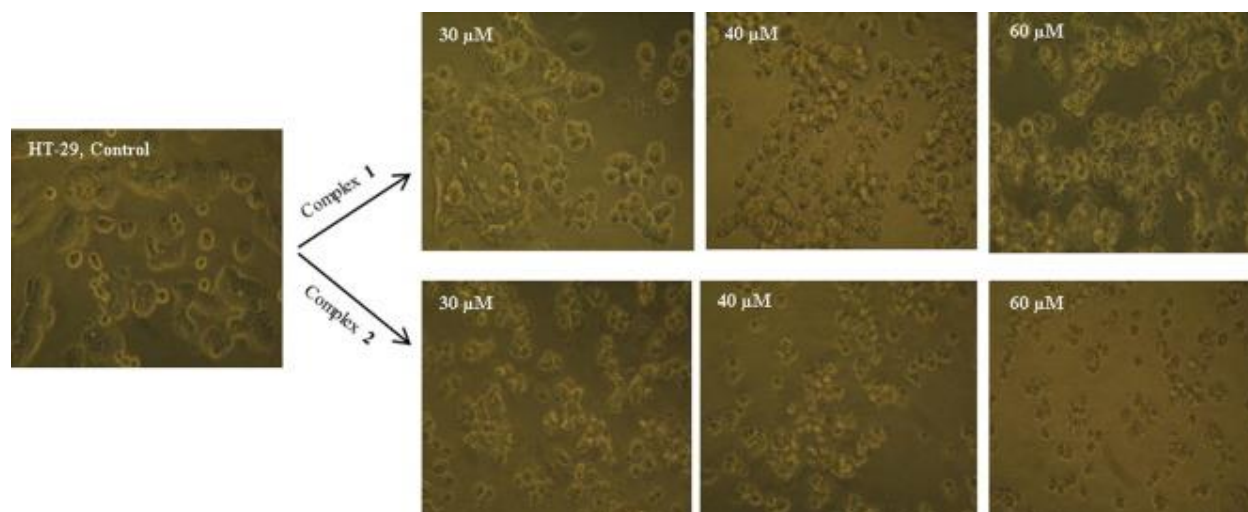


Fig. 19. The microscopic images of HT-29 cancer cells treated with the Cu(II) complexes at magnifications of 320 \times .

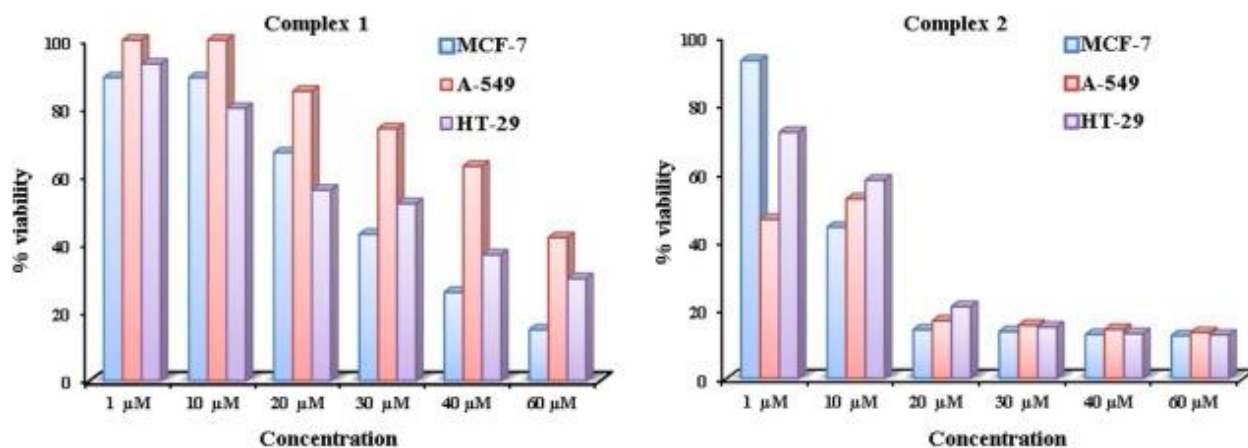


Fig. 20. Plots of percentage of viability vs. concentration of the Cu(II) complexes against of the MCF-7, A-549 and HT-29 cell lines.

Table 8. The IC₅₀ values (μM) obtained for the Cu(II) complexes against human cell lines.

Compound	MCF-7	A-549	HT-29
1	31	53	36
2	7.4	1.5	5.2
Cisplatin	9.6	16.4	22.8

4. Conclusion

Two mononuclear copper(II) complexes of 2,2'-bipyridine derivatives, [Cu(dimethoxybpy)₂](PF₆)₂ (**1**) and [Cu(dimethylbpy)₂Cl]PF₆ (**2**), have been prepared and fully characterized. The results of X-ray single crystal analysis indicate the coordination geometry of the complexes can be best described as distorted square-planar and distorted square-pyramidal structure, respectively. All interactions in crystal structures of **1** and **2** have been also studied by Hirshfeld surface analysis. Interaction studies of the complexes **1** and **2** with DNA suggest that the binding mode of them with DNA is partial intercalation binding. The results of electronic absorption, fluorescence titration, synchronous and CD show that the complexes also have high

binding affinity to BSA and change the secondary structure of the BSA. We propose that planar structure and hydrogen-bonding interactions, which would occur between the ligand in the complex **1** with DNA and BSA, would also contribute significantly to the higher DNA binding affinity of **1**. The results of molecular docking show hydrogen bonding between the methoxy group of **1** and base pairs of DNA and amino acids of BSA, which play significant role in stabilizing of the complex **1** interaction. The results obtained from MTT assay exhibit that the complex **2** has better cytotoxicity than the complex **1** under the same experimental conditions. This clearly indicates that the anticancer activity of the complexes is varies with the extent of their interaction with DNA. It is evident that the hydrophobic interaction of the methyl groups on the bpy rings in the complex **2** lead to its highest cytotoxicity.

Acknowledgments

We thank the head and director of the Institute of Science and High Technology & Environmental Sciences, Graduate University of Advanced Technology of Kerman.

Appendix A. Supplementary data

CCDC 1440772 contains the supplementary crystallographic data for [Cu(dimethoxybpy)₂](PF₆)₂ and 1433226 for [Cu(dimethylbpy)₂Cl]PF₆. These data can be obtained free of charge via <http://www.ccdc.cam.ac.uk/conts/retrieving.html>, or from the Cambridge Crystallographic Data Centre, 12 Union Road, Cambridge CB2 1EZ, UK; fax: (+44) 1223-336-033; or e-mail: deposit@ccdc.cam.ac.uk. Supplementary data associated with this article can be found, in the online version, at <http://dx.doi.org/10.1016/j.poly.2016.08.018>.

References

- [1] S.H. van Rijt, P.J. Sadler, *Drug Discov. Today* 14 (2009) 1089.
- [2] B. Rosenberg, L. Van Camp, J.E. Trosko, V.H. Mansour, *Nature* 222 (1969) 385.
- [3] S.M. Cohen, S.J. Lippard, *Prog. Nucleic Acid Res. Mol. Biol.* 67 (2001) 93.
- [4] P.C. Bruijninx, P.J. Sadler, *Curr. Opin. Chem. Biol.* 12 (2008) 197.

- [5] C. Santini, M. Pellei, V. Gandin, M. Porchia, F. Tisato, C. Marzano, *Chem. Rev.* 114 (2014) 815.
- [6] B.C. Bales, T. Kodama, Y.N. Weledji, M. Pitie, B. Meunier, M.M. Greenberg, *Nucleic Acids Res.* 33 (2005) 5371.
- [7] P. Uma Maheswari, S. Roy, H.D. Dulk, S. Barends, G.V. Wezel, B. Kozlevcar, P. Gamez, J. Reedijk, *J. Am. Chem. Soc.* 128 (2006) 710.
- [8] A. Barve, A. Kumbhar, M. Bhat, B. Joshi, R. Butcher, U. Sonawane, R. Joshi, *Inorg. Chem.* 48 (2009) 9120.
- [9] S. Ramakrishnan, D. Shakthipriya, E. Suresh, V.S. Periasamy, M.A. Akbarsha, M. Palaniandavar, *Inorg. Chem.* 50 (2011) 6458.
- [10] L. Ruiz-Azuara, United States Patent April 21, 1992, No. 5, 107, 005. US Patent Re 35, 458, February 18, 1997.
- [11] L. Ruiz-Azuara, United States Patent 1996, vol. 5576, 326.
- [12] L. Becco, A. Rodriguez, M.E. Bravo, M.J. Prieto, L. Ruiz-Azuara, B. Garat, V. Moreno, D. Gambino, *J. Inorg. Biochem.* 109 (2012) 49.
- [13] F. Carvallo-Chaigneau, C. Trejo-Solis, C. Gomez-Ruiz, E. Rodriguez-Aguilera, L. Macias-Rosales, E. Cortes-Barberena, C. Cedillo-Pelaez, I. Gracia-Mora, L. Ruiz-Azuara, V. Madrid-Marina, F. Constantino-Casas, *Biometals* 21 (2008) 17.
- [14] B.L. Fei, W. Li, W.S. Xu, Y.G. Li, J.Y. Long, Q.B. Liu, K.Z. Shao, Z.M. Su, W.Y. Sun, *J. Photochem. Photobiol. B: Biol.* 125 (2013) 32.
- [15] A. Jayamani, N. Sengottuvelan, S.K. Kang, Y.I. Kim, *Polyhedron* 98 (2015) 203.
- [16] V. Amani, A. Abedi, S. Ghabeshi, H.R. Khavasi, S.M. Hosseini, N. Safari, *Polyhedron* 79 (2014) 104.
- [17] T. Yamada, Y. Noguchi, M. Nakai, O. Yamauchi, Y. Nakabayashi, T. Sato, Y. Tamai, M. Chikuma, Y. Mino, *Inorg. Chim. Acta* 394 (2013) 190.
- [18] A.A. Shoukry, M.S. Mohamed, *Spectrochim. Acta Part A Mol. Biomol. Spectrosc.* 96 (2012) 586.
- [19] J. Marmur, *J. Mol. Biol.* 3 (1961) 208.
- [20] Oxford Diffraction Poland, CrysAlis CCD and CrysAlis Red, Version 1.171.33.42 (2009).
- [21] Bruker, APEX2, SAINT and SADABS, Bruker AXS Inc., Madison, Wisconsin, USA,

2008.

- [22] G.M. Sheldrick, *Acta Cryst. A* 71 (2015) 3.
- [23] G.M. Sheldrick, *Acta Cryst. C* 71 (2015) 3.
- [24] K. Brandenburg, H. Putz, DIAMOND Version 3.0, Crystal Impact GbR, Bonn, Germany (2006).
- [25] L.J. Farrugia, *J. Appl. Cryst.* 45 (2012) 849.
- [26] E. Keller, SCHAKAL99, University of Freiberg, Germany, 1999.
- [27] G. Cohen, H. Eisenberg, *Biopolymers* 6 (1968) 1077.
- [28] H.J.C. Berendsen, D. Van der Spoel, R. Van Drunen, *Comput. Phys. Commun.* 91 (1995) 43.
- [29] E. Lindah, B. Hess, D. Van der Spoel, *J. Mol. Model.* 7 (2001) 306.
- [30] W.F. Van Gunsteren, S.R. Billeter, A.A. Eising, P.H. Hünenberger, P.K.H.C. Krüger, A.E. Mark, W.R.P. Scott, I.G. Tironi, *Biomolecular Simulation: The GROMOS96 Manual and User Guide*, Vdf Hochschulverlag AG, Zürich, 1996.
- [31] W.F. Van Gunsteren, X. Daura, A.E. Mark, *Encyclopedia of Computational Chemistry*, Wiley and Sons, P. Von Rague Schleyer, Chichester, UK, 1998.
- [32] H.J.C. Berendsen, J.P.M. Postma, W.F. Van Gunsteren, J. Hermans, in: B. Pullman (Ed.), *Intermolecular Forces*, Reidel, Dordrecht, The Netherlands, 1981.
- [33] H.J.C. Berendsen, J.P.M. Postma, W.F. Van Gunsteren, A. Di Nola, J.R. Haak, *J. Chem. Phys.* 81 (1984) 3684.
- [34] T. Darden, D. York, L. Pedersen, *J. Chem. Phys.* 98 (1993) 10089.
- [35] U. Essmann, L. Perera, M.L. Berkowitz, T. Darden, H. Lee, L.G. Pedersen, *J. Chem. Phys.* 103 (1995) 8577.
- [36] G.M. Morris, D.S. Goodsell, R.S. Halliday, R. Huey, W.E. Hart, R.K. Belew, A.J. Olson, *J. Comput. Chem.* 19 (1998) 1639.
- [37] T.J. Mosmann, *J. Immunol. Methods* 65 (1983) 55.
- [38] M. Anjomshoa, S.J. Fatemi, M. Torkzadeh-Mahani, H. Hadadzadeh, *Spectrochim. Acta Part A Mol. Biomol. Spectrosc.* 127 (2014) 511.
- [39] L. Yang, D.R. Powell, R.P. Houser, *Dalton Trans.* (2007) 955.
- [40] A.W. Addison, T.N. Rao, J. Reedijk, J. van Rijn, G.C. Verschoor, *J. Chem. Soc., Dalton Trans.* (1984) 1349.

- [41] W.D. Harrison, D.M. Kennedy, M. Power, R. Sheahan, B.J. Hathaway, *J. Chem. Soc., Dalton Trans.* (1981) 1556.
- [42] P. Nagle, E. O'Sullivan, B.J. Hathaway, E. Muller, *J. Chem. Soc., Dalton Trans.* (1990) 3399.
- [43] C.L. Linfoot, P. Richardson, T.E. Hewat, O. Moudam, M.M. Forde, A. Collins, F. White, N. Robertson, *Dalton Trans.* (2010) 8945.
- [44] F.H. Li, D.Z. Gao, H.X. Wu, H.K. Lin, S.R. Zhu, *Jiegou Huaxue, Chin. J. Struct. Chem.* 23 (2004) 765–767.
- [45] A.M. Spackman, D. Jayatilaka, *Cryst. Eng. Comm.* 11 (2009) 19.
- [46] J.J. MacKimon, M.A. Spackman, A.S. Mitchell, *Acta Crystallogr. Sect. B: Struct. Sci.* 60 (2004) 627.
- [47] J.J. MacKimon, D. Jayatilaka, A.M. Spackman, *Chem. Commun.* 37 (2007) 3814.
- [48] S.K. Wolff, D.J. Grimwood, J.J. MacKimon, M.J. Turner, D. Jayatilaka, A.M. Spackman, *Crystal Explorer ver. 3.1*, University of Western Australia, Perth, Australia, 2013.
- [49] Z.F. Chen, Y.F. Shi, Y.C. Liu, X. Hong, B. Geng, Y. Peng, H. Liang, *Inorg. Chem.* 51 (2012) 1998.
- [50] J.K. Barton, A.T. Danishefsky, J.M. Goldberg, *J. Am. Chem. Soc.* 106 (1984) 2172.
- [51] A. Wolfe, G.H. Shimer, T. Meehan, *Biochemistry* 26 (1987) 6392.
- [52] S. Ramakrishnan, D. Shakthipriya, E. Suresh, V.S. Periasamy, M. Abdulkader Akbarsha, M. Palaniandavar, *Inorg. Chem.* 50 (2011) 6458.
- [53] M. Anjomshoa, H. Hadadzadeh, M. Torkzadeh-Mahani, S.J. Fatemi, M. Adeli-Sardou, H. Amiri Rudbari, V.M. Nardo, *Eur. J. Med. Chem.* 96 (2015) 66.
- [54] M. Anjomshoa, M. Torkzadeh-Mahani, *Spectrochim. Acta Part A Mol. Biomol. Spectrosc.* 15 (2015) 390.
- [55] J.R. Lakowicz, *Principles of Fluorescence Spectroscopy*, 2nd ed., Plenum Press, New York, 1999.
- [56] M. Anjomshoa, H. Hadadzadeh, S.J. Fatemi, M. Torkzadeh-Mahani, *Spectrochim. Acta Part A Mol. Biomol. Spectrosc.* 136 (2015) 205.
- [57] P.D. Ross, S. Subramanian, *Biochemistry* 20 (1981) 3096.
- [58] J.M. Veal, R.L. Rill, *Biochemistry* 30 (1991) 1132.

- [59] Biotium. <<http://www.biotium.com>>, 2013 (accessed Oct 2014).
- [60] Q. Huang, L. Baum, W.L. Fu, *Clin. Lab.* 56 (2010) 149.
- [61] M. Anjomshoa, M. Torkzadeh-Mahani, *J. Fluoresc.* 26 (2016) 1505.
- [62] D. Suh, J.B. Chaires, *Bioorg. Med. Chem.* 3 (1995) 723.
- [63] D.L. Boger, B.E. Fink, S.R. Brunette, W.C. Tse, M.P. Hedrick, *J. Am. Chem. Soc.* 123 (2001) 5878.
- [64] W. Saenger (Ed.), *Principles of Nucleic Acids Structure*, Springer-Verlag, New York, 1988. 350.
- [65] L. Messori, P. Orioli, C. Tempì, G. Marcon, *Biochem. Biophys. Res. Commun.* 281 (2001) 352.
- [66] S. Mahadevan, M. Palaniandavar, *Inorg. Chem.* 37 (1998) 693.
- [67] M.T. Carter, M. Rodriguez, A.J. Bard, *J. Am. Chem. Soc.* 123 (1989) 8901.
- [68] H. Polet, J. Steinhardt, *Biochemistry* 7 (1968) 1348.
- [69] G. Zhang, Y. Ma, L. Wang, Y. Zhang, J. Zhou, *Food Chem.* 133 (2012) 264.
- [70] Y.Q. Wang, H.M. Zhang, G.C. Zhang, W.H. Tao, S.H. Tang, *J. Lumin.* 126 (2007) 211.
- [71] J.G. Da Silva, A.A. Recio Despaigne, S.R.W. Louro, C.C. Bandeira, E.M. Souza-Fagundes, H. Beraldo, *Eur. J. Med. Chem.* 65 (2013) 415.
- [72] B.A. Wallance, J.G. Lees, A.J.W. Orry, A. Lobley, R.W. Janes, *Protein Sci.* 12 (2003) 875.
- [73] A.R. Timerbaev, C.G. Hartinger, S.S. Aleksenko, B.K. Keppler, *Chem. Rev.* 106 (2006) 2224.